Biomaterials Advances 177 (2025) 214408

Contents lists available at ScienceDirect

Biomaterials Advances

journal homepage: www.journals.elsevier.com/materials-science-and-engineering-c

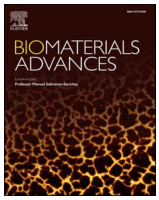

Gelatin *vs* GelMA in alginate-based bioinks as a platform for versatile 3D bioprintable *in vitro* systems

Alvaro Sanchez-Rubio [a], Lauren Hope [a,b], Eva Barcelona-Estaje [a], Vineetha Jayawarna [a], Jonathan Williams [c], Manuel Salmeron-Sanchez [a,d,e,*]

[a] *Centre for the Cellular Microenvironment, University of Glasgow, United Kingdom*
[b] *Paul O'Gorman Leukaemia Research Centre, University of Glasgow, United Kingdom*
[c] *Department of Biomedical Engineering, University of Strathclyde, United Kingdom*
[d] *Institute for Bioengineering of Catalonia (IBEC), The Barcelona Institute for Science and Technology (BIST), 08028 Barcelona, Spain*
[e] *Institució Catalana de Recerca i Estudis Avançats (ICREA), Barcelona, Spain*

ARTICLE INFO

Keywords:
Alginate
Gelma
Bioprinting
Stem cells
Endothelial cells

ABSTRACT

3D *in vitro* model systems, such as hydrogels, have garnered popularity due to their ability to more accurately recapitulate *in vivo* environments compared to 2D cell culture systems. However, methods which involve casting hydrogels by hand may be time consuming, have poor reproducibility, and reduced capacity to generate complex structures. Hence, 3D bioprinting has emerged as a useful tool for the high throughput production of *in vitro* tissue models such as hydrogels and complex constructs. Here, we demonstrate the mechanical properties, printability, and ability to support single cells and spheroids in culture for two highly characterised composite bioinks: Alginate/Gelatin (AlgGel), which is ionically crosslinked, and Alginate/Gelatin Methacrylate (GelMA) (AlgGelMA), whereby the GelMA is crosslinked by illumination with UV light. In this study, we engineered gels that exhibit a wide range of stiffnesses, which vary due to the concentration of crosslinking polymer present. AlgGel hydrogels were softer (1.5–4.5 kPa), and stiffness decreased with time in culture, however, AlgGelMA hydrogels were stiffer (6–40 kPa), and the stiffness increased with time. Microarchitectural studies using Scanning Electron Microscopy and Microcomputed Tomography (μCT) revealed that hydrogels produced using both bioinks bore a highly porous structure, further simulating *in vivo* conditions. To assess the ability of both bioink families to support cell culture, the Acute Myeloid Leukaemia cell line THP-1 and human Mesenchymal Stem Cells (hMSCs) as single cells and spheroids were bioprinted in each bioink. Interestingly, THP-1 cells formed larger clusters when cultured within AlgGel bioinks compared to AlgGelMA. Additionally, hMSCs appeared to be unable to migrate through the AlgGel matrix, as single hMSCs displayed rounded morphologies and hMSC spheroid shape was not disrupted after seven days. Contrastingly, hMSCs and spheroids cultured within AlgGelMA hydrogels were able to invade the gel matrix and migrate. Together, these data demonstrate that both AlgGel and AlgGelMA bioinks show promise for use as the basis of 3D bioprinted *in vitro* tissue models.

1. Introduction

In vitro engineered constructs allow biological systems to be systematically studied within a controlled environment. Often, this includes materials with known physical and chemical properties, where a multitude of features such as the presence of adhesion ligands, the degradability, or the stiffness can be engineered, and are used to drive or enhance specific cell behaviours ([1,2]). Nevertheless, *in vitro* models exhibit a spectrum of complexity, ranging from foundational 2D cell culture models that have significantly advanced our comprehension of biological systems, to more intricate 3D models that aim to replicate the environment of native tissues and can incorporate biomaterials. Hence, models that provide this 3D environment, such as hydrogels, have been developed [3–6]. Generally, the closer a model can replicate the native tissue, the closer the predicted response will be. In fact, some current models include multiple heterogeneous regions within a single construct [7]. However, traditional 3D fabrication techniques can be time-consuming, inefficient, pose reproducibility challenges, and require

* Corresponding author at: Centre for the Cellular Microenvironment, University of Glasgow, United Kingdom.
E-mail address: manuel.salmeron-sanchez@glasgow.ac.uk (M. Salmeron-Sanchez).

https://doi.org/10.1016/j.bioadv.2025.214408
Received 3 March 2025; Received in revised form 18 June 2025; Accepted 8 July 2025
Available online 9 July 2025

highly trained personnel to perform every step of the process. Recently, bioprinting technology has enabled fabrication of 3D constructs with predetermined geometries. This has enabled improved replication of the biological system under study, by matching both material properties (*e.g.* by using bioinks) and architectural features. Moreover, bioprinting provides a computer-aided approach to biofabricating these models, thereby automating the production process, mitigating human error, increasing reproducibility and repeatability, and allowing scalability [8,9].

3D bioprinting uses bioinks (cell-laden hydrogels) as the printing material that provides a 3D extracellular matrix (ECM)-like environment. These bioinks can be natural (like alginate, gelatine or hyaluronic acid ([10,11]; Z. [12–14]), synthetic (like polyethylene glycol (PEG) or Pluronic [15,16], or derived from tissue-specific decellularised extracellular matrix [17], each entailing their own advantages and disadvantages. For example, natural bioinks are considered to be inherently biocompatible, however, they can carry some immunogenicity and can trigger interactions between cells and materials which may be difficult to isolate. Synthetic bioinks are fully defined but they have been associated with lower cell viability due to toxic by-products [18,19]. These bioinks can be functionalised using additional proteins, domains and growth factors. Such cues, both physical and chemical, provide cells with an environment much closer to that of native tissues and are crucial in driving certain behaviours and phenotypes [20].

However, bioinks (especially those utilised for extrusion-based bioprinting applications) need to be printable with suitable accuracy, while allowing cells to remain viable. Rheological properties, such as viscosity or shear-thinning behaviour; print parameters including print time, usable nozzle gauge or printing temperature; and post-processing conditions such as the crosslinking method used will influence the suitability of potential bioink formulations [21–23].

Alginate/gelatine-based bioinks have been studied previously and are widely accepted as bioink models due to their ability to support cell viability, while equally offering good printability [24,25]. Both alginate and gelatine confer desirable features: alginate is bioinert but increases the viscosity and improves the printability of the bioink [26], while gelatine provides further viscosity control based on its temperature-sensitivity and shear-thinning properties, and provides relevant domains like cell or ECM-binding sites ([27]; X. [28]). However, previous research has not focused on the effect of selectively crosslinking either network within them (alginate or gelatine), thereby failing to show the complete potential of these bioink families to span a broad range of properties. Similarly, different cell types and conformations require different 3D culture conditions to better model their native environment. Cell-adhesive features as well as mechanical properties can lead to highly different biological responses. In fact, adhesion ligands have been previously used in tissue engineering to modulate different biological processes, guide differentiation, or promote migration [29–31]. For instance, adhesion ligands are closely related to cancer dynamics, tumour progression and metastasis [29]. Nevertheless, adhesion ligands (or lack thereof) can also be used to control biological processes like stemness [32], or to maintain cells in a quiescent state [33]. This is similar for adherent and suspension cells in *in vitro* conditions. Suspension cells such as haematopoietic stem cells and leukaemic blasts cultured within 3D environments, such as hydrogels or spheroid co-culture, display behaviours more analogous to *in vivo* conditions. These include migration [34], increased chemotherapy resistance compared to 2D culture [35], and stemness, whereby the presence or absence of cell-binding ligands can promote stemness maintenance or differentiation [36]. Together, this highlights the importance of developing humanised 3D culture systems to mimic healthy and diseased tissue states.

Further, to appropriately mimic biological systems, mechanical properties need to be considered too. For example, the bone marrow provides a softer environment, while cortical bone possesses much higher mechanical stiffness [37]. We show that both alginate/gelatine bioink families are highly tuneable and are suitable for a wide range of applications. Such applications could include bone regeneration [38], and *in vitro* modelling of organs including vasculature, lung, heart, and multicellular systems such as organoids or spheroids [7,39].

In this work we introduce two families of AlgGel-based bioinks that offer highly controlled physicochemical properties, such as stiffness, degradability, or network microarchitecture, by selectively crosslinking one of the polymer networks. Likewise, the bioinks possess different cell-instructive properties and confer clear distinctive 3D environments in which different processes, involving both non-adherent and adherent cell types, as well as multicellular conformations, can be studied.

2. Materials and methods

2.1. Preparation of alginate/gelatine hydrogels

Sodium alginate (Sigma Aldrich, United Kingdom) and gelatine type A (Gel strength: 300; Sigma Aldrich, United Kingdom) powders were used to make hydrogels of 1 % alginate/8 % gelatine and 2 % alginate/8 % gelatine. 1.5× desired concentration was measured per powder. Alginate powder was dissolved in sterile PBS at 37 °C. Gelatine was then added under sterile conditions. The mixture was incubated at 37 °C until the gelatine powder had fully dissolved.

For use in experiments, the gel was diluted by one third using media or PBS to achieve the desired concentration. 100 μL of gel solution was added per sample within either a 24-well plate or polystyrene Petri dish. Gels were submerged in 150 mM calcium chloride (Sigma Aldrich, United Kingdom) solution for 10 min. The gels were washed with PBS then media. The gels were incubated at 37 °C.

2.2. Preparation of alginate/gelatine-methacryloyl (GelMA) hydrogels

Sodium alginate (Sigma Aldrich) powder and GelMA (degree of substitution: 80 %; Gelomics, Australia) were used to make composite hydrogels of 2 % alginate with either 6 % or 9 % GelMA. Sodium alginate was dissolved in sterile PBS to make a final concentration of 2 % alginate. Lyophilised GelMA was reconstituted in 5 mL PBS (final concentration: 20 % (*w/v*)) and incubated at 35 °C until fully dissolved. Alginate, GelMA and PBS were added to a 2 mL Eppendorf tube (Gibco) to make the desired concentrations. The Eppendorf was then incubated briefly at 37 °C. After 5 min, the photoinitiator Lithium Phenyl-2,4,6-trimethylbenzoylphosphinate (LAP) was added to the gel, to a final concentration of 2 mM. Polydimethylsiloxane (PDMS) moulds of either 50 μL or 100 μL were rinsed with water, blotted dry, then sterilised with ethanol prior to use. The gel was mixed, then cast into the mould. The gels were then irradiated with UV light (365 nm, Omnicure S2000, Excelitas) for 7 min at 7 mW/cm^2 to enable GelMA crosslinking.

2.3. Swelling and degradation analysis

Alginate/gelatine and alginate/GelMA hydrogels of the selected concentrations (described above) were cast in pre-weighed Eppendorf tubes. To assess swelling, gels were submerged in 1 mL of media; to evaluate gel degradation, gels were submerged in collagenase 1 (50 U/mg in saline water) to assess gelatine degradation, or PBS to target calcium crosslinking of alginate. Gels were then incubated at 37 °C. At each timepoint, the supernatant was removed from the Eppendorf and the tubes containing the gels were weighed. The tubes were then replenished with fresh media, collagenase or PBS and incubated at 37 °C. Swelling and degradation were assessed as the percentage increase and decrease, respectively.

2.4. Scanning electron microscopy

Scanning electron microscopy (SEM) was used to visualise the microstructure of selected concentrations of alginate/gelatine and

alginate/GelMA hydrogels. Alginate/gelatine and alginate/GelMA gels were made as described above. Gels were lyophilised by submerging in liquid nitrogen for approximately 30–60 s then freeze-drying at −80 °C at 0 Bar for 24 h (Labconco).

Freeze-dried gels were then sliced in half using a razor to obtain cross-sections and sputter-coated with gold prior to SEM. SEM was completed using the JEOL IT 100 Scanning Electron Microscope running at 10 kV, and images taken at 300× and 2000× using INTOUCH Scope software (version 1.05). Pore size was measured in Fiji (ImageJ), by measuring the length and width of each pore in each 300× image ($n = 6$ per gel composition), and calculating the approximate area using the area of an ellipse:

$$Area_{Ellipse} = \pi ab$$

2.5. Micro-computed tomography

The structure of lyophilised AlgGelMA hydrogels (described above) was further examined with micro-computed tomography (Skyscan 1172, Bruker) at a voxel size of 2.5 μm. All scans were performed at a tube voltage 43 kVp, 100 μA tube current, 1000 ms exposure time, 0.3° rotation step (180° total), without a metal filter and with frame averaging set to 2. Scans were then reconstructed into 8-bit grayscale images using Skyscan NRecon software (Bruker, version 1.6.9.18). A centrally located rectangular sub-volume of interest (SubVOI) within each scanned hydrogel, of side lengths 0.75 mm × 2.5 mm × 1.875 mm, was selected for 3D morphometric analysis in CTAn software (version 1.20.8). SubVOIs were binarised using a global threshold (40–255) and denoised (removal of black speckles smaller than 20 voxels and white speckles <80 voxels). The morphometric parameters porosity (%), average gel fibre and pore thickness (μm) and their distributions calculated using the maximum sphere fitting algorithm, and connectivity density (mm^{-3}) were calculated in CTAn.

2.6. Rheological properties of alginate/gelatine and alginate/GelMA hydrogels

Alginate/gelatine and alginate/GelMA gel stocks were warmed as described above. Gels were cast into 16 mm diameter moulds and incubated at 37 °C for 1 h or two days. Rheology was completed using the Modular Compact Rheometer (MCR) 302 (Anton Paar) fitted with a parallel plate PP15 (Anton Paar). The platform was heated to 37 °C, matching physiological temperature. To ensure appropriate contact with the parallel plate, a pre-compression of 25 % of the initial gel height was used. The linear viscoelastic region was first identified using a strain sweep, at a normal force of 0.5–1 N and an angular frequency of 10 rad/s. Next, amplitude sweeps were performed within this linear viscoelastic region, between a strain rate of 0.1–1 % strain rate at a constant frequency of 10 rad/s. The Young's Modulus (E) was then calculated:

$$E = 2(1 + \nu)G'$$

2.7. Cell culture

Human mesenchymal stem cells (hMSCs) (Promocell, Germany) were maintained in Dulbecco's Modified Eagle Medium (DMEM) containing 10 % foetal bovine serum (FBS), 5 % antibiotic mix (penicillin and streptomycin) (Gibco, United Kingdom), 1 % non-essential amino acids (Gibco, United Kingdom), and 1 % sodium pyruvate (Gibco, United Kingdom). Human acute monocytic leukaemia cell line THP-1 was cultured in Roswell Park Memorial Institute (RPMI) 1640 media (Gibco) with 20 % FBS (Gibco), supplemented with L-glutamine (2 mM), penicillin (100 U/mL) and streptomycin (100 g/mL).

2.8. Generation of mesenchymal stem cell spheroids

hMSC spheroids were generated using 24-well (1200 microwells) low-adherence AggreWell™400 Microwell Culture Plates (Stem Cell Technologies), as per manufacturer's instructions. hMSCs were seeded at 100 cells per microwell, and incubated at 37 °C for 24 h to allow spheroid formation. Spheroids were then harvested as per manufacturer's instructions. Single cells were removed by passing harvested spheroids through a 37 μm cell strainer.

2.9. 3D bioprinting of alginate/gelatine and alginate/GelMA bioinks

3D bioprinting was completed using the RegenHU 3D Discovery (RegenHU, Switzerland). Gel constructs and G codes were designed using BioCAD™ software (Supplementary fig. 1), and the STL files generated were sliced using BioCAM™ software (RegenHU, Switzerland). Alginate/Gelatine and Alginate/GelMA hydrogels were prepared as above. The cartridge containing the gel was maintained at 37 °C until printing. Gels were printed using a 22 G needle (Nordson EFD, USA/Canada), then crosslinked as outlined above.

2.10. Single material structures

Lattice structures were printed at a thickness of 0.1 mm, with a printing speed of 10 mm/s. These structures were printed with 45°/−45° stripe pattern, and various infills. Microgels were printed using 0.5–1 shots per gel. Hollow tube structures were printed at a thickness of 0.15 mm, and a printing speed of 12 mm/s. These structures were generated by extruding 70 layers of 9 mm circles, with perpendicular infill lines between layers. After crosslinking, the infill lines were excised using surgical scissors. Anatomically based structures were generated by producing an STL file on parametric design software, then this file was opened using BioCAM™ software. Cell-free constructs were extruded at a pressure below 150 kPa.

2.11. Multiple material structures

Multiple materials structures are composed of two or more materials, containing different polymers, cells or proteins. These structures were printed at a thickness of 0.15 mm, and a printing speed of 12 mm/s. Pore-drop loaded structures were generated through printing one lattice and subsequently printing a series of microgels (both as described above), which fit within the infills of the lattice structure.

2.12. Cell-laden bioinks

THP-1 cells, hMSCs and hMSC spheroids were added to the Alginate/Gelatine or Alginate/GelMA hydrogels as described above, at concentrations of 2×10^6 cells/mL, 2×10^6 cells/mL, and 2×10^3 spheroids/mL, respectively. Alginate/Gelatine gels were extruded at 30–40 kPa and Alginate/GelMA gels were extruded at 10–20 kPa. Gel structures were 6 mm in diameter. These were printed at a speed of 0.12 mm/s and thickness of 0.1 mm.

2.13. Assessment of cell viability using live/dead staining

Cell viability was determined using the LIVE/DEAD™ Viability/Cytotoxicity Kit (Invitrogen™). Gels were washed in prewarmed PBS, then Calcein-AM (2 mM) and Ethidium Homodimer-1 (4 mM) were added. Gels were protected from light using aluminium foil, and incubated at 37 °C for 15–30 min. Gels were washed in warm PBS and imaged on the EVOS M7000 Imager (Invitrogen™) at 10× and 20× magnification (Ex/Em: Calcein AM: 494/517 nm; Ethidium Homodimer-1: 517/617 nm). Analysis was completed using ImageJ by thresholding each image, counting the number of Calcein-AM positive cells and Ethidium Homodimer-1 positive cells, and obtaining a

percentage viability.

2.14. Investigating cell morphology using rhodamine phalloidin/DAPI staining

Cell morphology was investigated using Rhodamine Phalloidin (F-Actin) and DAPI (nuclei) staining. Alginate/gelatine and alginate/GelMA hydrogels containing THP-1 cells, hMSCs or hMSC spheroids were fixed in 4 % paraformaldehyde in PBS at 37 °C for 15 min. Gels were washed with PBS then submerged in permeabilisation solution (10.3 g sucrose, 0.292 g sodium chloride, 0.06 g magnesium chloride (hexahydrate), 0.476 g HEPES in 100 mL PBS, 0.5 mL Triton X) and incubated at 4 °C for 5 min. Gels were washed with PBS. Gels were covered in 1 % bovine serum albumin (BSA) and incubated for 5 min at 37 °C. ActinGreen™ 488 ReadyProbes™ Reagent (AlexaFluor™ 488 phalloidin) (Thermo Fisher Scientific, United Kingdom) was diluted in 1 % BSA and added to each gel. The gels were shielded from light using aluminium foil, and were incubated for 15–30 min at 37 °C. After incubating, the gels were placed on a shaker and briefly washed three times with 0.5 % PBS-Tween20. Gels were added to microscope slides (VWR International), and VECTASHIELD Antifade mounting media with DAPI (Vector Laboratories, USA) was added to each gel. Images were taken using the EVOS M7000 Imager (Invitrogen, United Kingdom) at 10× and 20× magnification (Ex/Em: ActinGreen: 495/518 nm; DAPI: 360/460 nm).

2.15. Statistical analysis

Statistical analyses were carried out using GraphPad Prism software (versions 6.2 and 9.5.1). All experiments were carried out with at least three replicates. Unless specified, data is represented as the mean ± standard deviation. Data was first assessed using D'Agostino-Pearson or Shapiro-Wilk (SEM data) normality test to determine normality of distribution. Where two groups were compared, unpaired *t*-tests were used; for analysis of three or more groups, One-way ANOVAs followed by Tukey's post-hoc tests were used for normally distributed datasets. For non-normally distributed datasets, Mann Whitney *U* tests were selected when comparing two groups, whilst Kruskal-Wallis tests were performed on datasets whereby three or more groups were compared. Statistical significance was classified as $*P < 0.05$, $**P < 0.01$, $***P < 0.001$, $****P < 0.0001$.

3. Results

3.1. Alginate/gelatine and alginate/GelMA-based bioinks

Alginate Gelatine (AlgGel) bioinks are made from an uncrosslinked solution that comprises alginate and gelatine. Alginate is ionically crosslinked by submergence in $CaCl_2$ solution, which allows Ca^{2+} ions to integrate into the network and bind with L-Guluronic acid (G) groups of neighbouring alginate chains, forming a hydrogel. Gelatine is not crosslinked, and is released from the gel when incubated at 37 °C. Thereby the resulting network lacks the gelatine-provided sites for cell attachment.

Alginate GelMA (AlgGelMA) bioinks are made from a mixture of two hydrogel solutions, one containing alginate and the other containing Gelatin Methacryloyl (GelMA), at selected ratios. GelMA is made by the reaction of gelatine with methacrylic anhydride, resulting in the addition of methacrylate residues on gelatine polymers [40]. This enables the methacrylate residues within the network to be UV-crosslinked. This process involves the addition of the photoinitiator lithium phenyl-2,4,6-trimethylbenzoylphosphinate (LAP), which creates free radicals in the presence of UV light, initiating photopolymerisation [41]. The network is formed by the GelMA molecules only, the alginate is not crosslinked, but rather entrapped into the network. AlgGelMA is a highly tuneable hydrogel network that maintains the bioactivity of gelatine *i.e.* cell adhesion capabilities, degradability due to presence of matrix metalloprotease (MMP) cleavable sites, and binding to ECM proteins like fibronectin [27,42].

Both AlgGel and AlgGelMA bioinks exhibit temperature-dependent viscosity, provided by gelatine. Alginate and gelatine are negatively charged, their presence in a hydrogel can provide a sustained release of positively charged proteins, such as growth factors ([43,44]). Contrary to AlgGel hydrogels, AlgGelMA hydrogels are formed of a gelatine network, therefore presenting cell binding sites. Schematic representations of gelatine, alginate and GelMA, and resulting crosslinked bioinks are shown in Fig. 1A, while Fig. 1B illustrates how these bioinks are integrated into bioprinting.

3.2. Fabrication of different structures using AlgGel and AlgGelMA bioinks

The suitability of AlgGel and AlgGelMA bioinks as biomaterials for a wide range of printing applications was demonstrated by their ability to produce a myriad of single and multiple materials structures (Fig. 1C-J). Firstly lattices, which are widely used as a testament of bioprinting capabilities ([45–47]), were fabricated using both AlgGel and AlgGelMA bioinks. In both cases, printed constructs showed clearly defined pores and sharp edges, which are indicators of printing accuracy (Fig. 1C). To exploit the automation and reproducible capabilities of 3D bioprinting, droplet microgel arrays were fabricated, displaying fast and human-error-free production of controllable size 3D hydrogel constructs (Fig. 1D). Anatomically based structures produced using AlgGel bioinks showed good representation of architectural features such as the ear lobe, concha, tragus and helix (Fig. 1E). Similarly, hollow tubes (vessels) were printed up to a height of 1 cm, composed of 3 concentric layers (Fig. 1F). The last two approaches demonstrate specific, tissue-mimicking architectures.

Following this, several constructs which included more than one material were bioprinted to highlight the potential of these bioinks for multi-material tissue construct and model applications. Horizontal patterns (z axis = 0) were explored in a lattice and solid form, both showing a clear distinction between the different areas (Fig. 1G-J). Fabricating these types of architectures is of great interest as it grants the possibility of replicating the heterogeneity present in tissues and organs, and has been used to produce models [48] and implantable tissue constructs [49].

The next type of multi-material structure created were pore-drop loaded constructs, whereby a second bioink was dropped into the pores of the first bioink lattice (Fig. 1I). This approach allows construction of patterned bioinks that possess highly relevant chemical and/or biological features, but are not printable enough to be used in bioprinting. The different crosslinking methods used by both AlgGel and AlgGelMA bioink families, and the reversible gelation of gelatine, *i.e.* gelatine adopts a gel-like state at room temperature while a liquid-like state at 37 °C, can also be utilised to produce multiple material constructs. Specifically, to produce perfusable constructs that possess empty channels from which liquid (typically this involves media which contains cytokines, nutrients and vessel lining cells) can flow through. To do so, a sacrificial AlgGel branched structure can be printed on top of an AlgGelMA slab, then covered with more AlgGelMA and crosslinked using UV light. The AlgGel construct would then possess an uncrosslinked geometry that will leak out when placed at cell culture conditions (Fig. 1H). Such constructs, which enable perfusion of solutions such as media, have been widely used in *in vitro* models and tissue engineering to circumvent issues caused by the lack of nutrients and oxygen in multicellular systems, and to model native tubular structures such as vasculature [50–52].

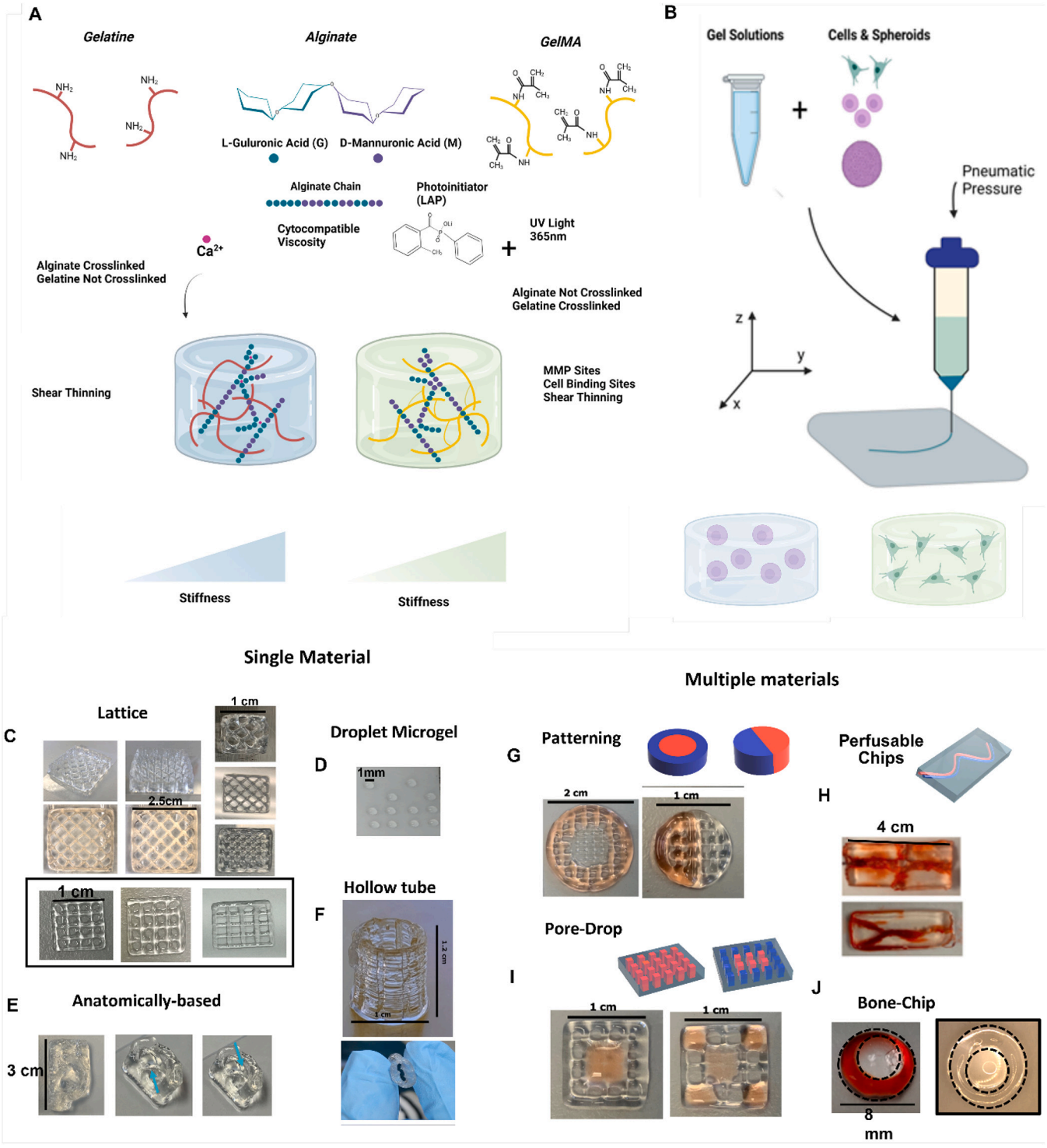

Fig. 1. AlgGel and AlgGelMA bioinks. A) Diagram showing AlgGel (blue) and AlgGelMA (green) bioink chemistry, hydrogel formation mechanism. B) Diagram showing the incorporation of adherent cells (green), suspension cells (lilac) and spheroids (purple) into a bioink and how bioprinting works. Examples of printed single material (C-F) and multiple material constructs (G-J). 3D bioprinted constructs within the black box were produced using AlgGelMA (C), and the remainder were fabricated using AlgGel. Construct designs and reference dimensions are available in supplementary fig. 1.

3.3. Viscosity and printability characterisation of AlgGel and AlgGelMA-based bioinks

The rheological properties of the bioinks, both in varying temperature and polymer concentration conditions will greatly influence the printing conditions. For instance, the pressure required to print each of the different bioinks can be linked to their viscosity. Gelatine-based bioinks exhibit a phase-transition between solid and fluid states, which results in a sharp increase in viscosity when using both gelatine (Supplementary fig. 2A) and GelMA (Supplementary fig. 2B). Although Alginate (Alg) bioinks do not exhibit the sharp increase in viscosity (Supplementary fig. 2C) at decreasing temperatures, the addition of alginate to the bioinks had an important contribution over the bioink properties, providing a viscosity 10-times higher than Gelatin (Gel) only

(Supplementary fig. 2A) or GelMA-only (Supplementary fig. 2B) counterparts. The effect of alginate addition to bioinks have been studied previously, where alginate was shown to provide a higher tan(δ) which resulted in lower lateral-diffusing bioinks [26]. Similarly, increasing the concentration of both polymers resulted in higher viscosities in AlgGel (Fig. 2B) and AlgGelMA (Fig. 2E) bioinks. In supplementary fig. 2D the viscosities of the different formulations depending on temperature can be seen, highlighting the differences between the Alg-only and Gel-based bioinks.

Printability of different formulations of both bioink families was also tested. First, the minimum pressure required to extrude each bioink at specific temperature was measured (Fig. 2C). Second, constructs containing challenging geometries (sharp edges, straight lines and small angles) were printed at 37 °C, and their respective required pressures, for all bioinks (Fig. 2F & G). It has been discussed in literature how higher shear stresses, often coming from smaller needle diameters and higher pressures, result in higher cell death [23]. From the printability assessment performed, all bioinks were printable at below 20 kPa and 37 °C, and all were able to produce constructs with sharp edges and straight lines. In addition, printing at 37 °C not only reduces the required printing pressure but also provides physiological conditions for cells.

3.4. Swelling and degradability of AlgGel and AlgGelMA hydrogels

AlgGel bioinks increased in weight when incubated in collagenase (Fig. 3A), indicating uptake of the solution and therefore swelling with no signs of degradation, *i.e.* the absence of MMP-cleavable sites in alginate prevents degradation of the gel. In all conditions, no significant differences were found between selected gel formulations. AlgGel bioinks displayed a 100 % weight increase within the first 4 h when incubated in media, however, by 72 h this had reduced to less than the original weight (Fig. 3B). This subsequent decrease could be explained by uncrosslinked gelatine exiting the gel, and by the presence of PO_4^{3-} ions in media (K. Y. [53]), which sequester the Ca^{2+} ions in the alginate, therefore disturbing the network. AlgGel bioinks degraded completely in DPBS within 24 h (Fig. 3C). DPBS contains negatively charged ions including PO_4^{3-} and Cl^-, which disrupt the ionic crosslinks.

Contrary to AlgGel, AlgGelMA bioinks degraded completely within seven days when maintained in collagenase solution, with the lower GelMA concentration (6 %) degrading sooner than the higher concentration (9 %) hydrogels (Fig. 3D). Gelatine-based hydrogels such as AlgGelMA contain MMP-cleavable sites and can therefore be degraded by MMPs such as collagenase [54]. Interestingly, AlgGelMA bioink weight initially increased, then remained constant (within ±20 % of the initial weight) when submerged in media and DPBS (Fig. 3E & F). As AlgGelMA is not ionically crosslinked, the ions within DPBS and media cannot interfere with the hydrogel network.

3.5. Mechanical properties of AlgGel and AlgGelMA hydrogels

AlgGel hydrogels containing higher alginate concentrations displayed a higher storage modulus, and therefore Young's modulus compared to lower alginate concentrations (Fig. 3G). This could be explained by the higher network density shown later in this work. However, the storage modulus decreased for all conditions after two days (Fig. 3H), which could be due to disruption of the Ca^{2+} crosslinking caused by the ions present in the cell culture media. To examine this further, AlgGel2%8 % hydrogels were crosslinked for 10, 20 or 30 min. No significant differences were found in storage modulus at day 0 (Fig. 3I). However, after two days it was apparent that longer

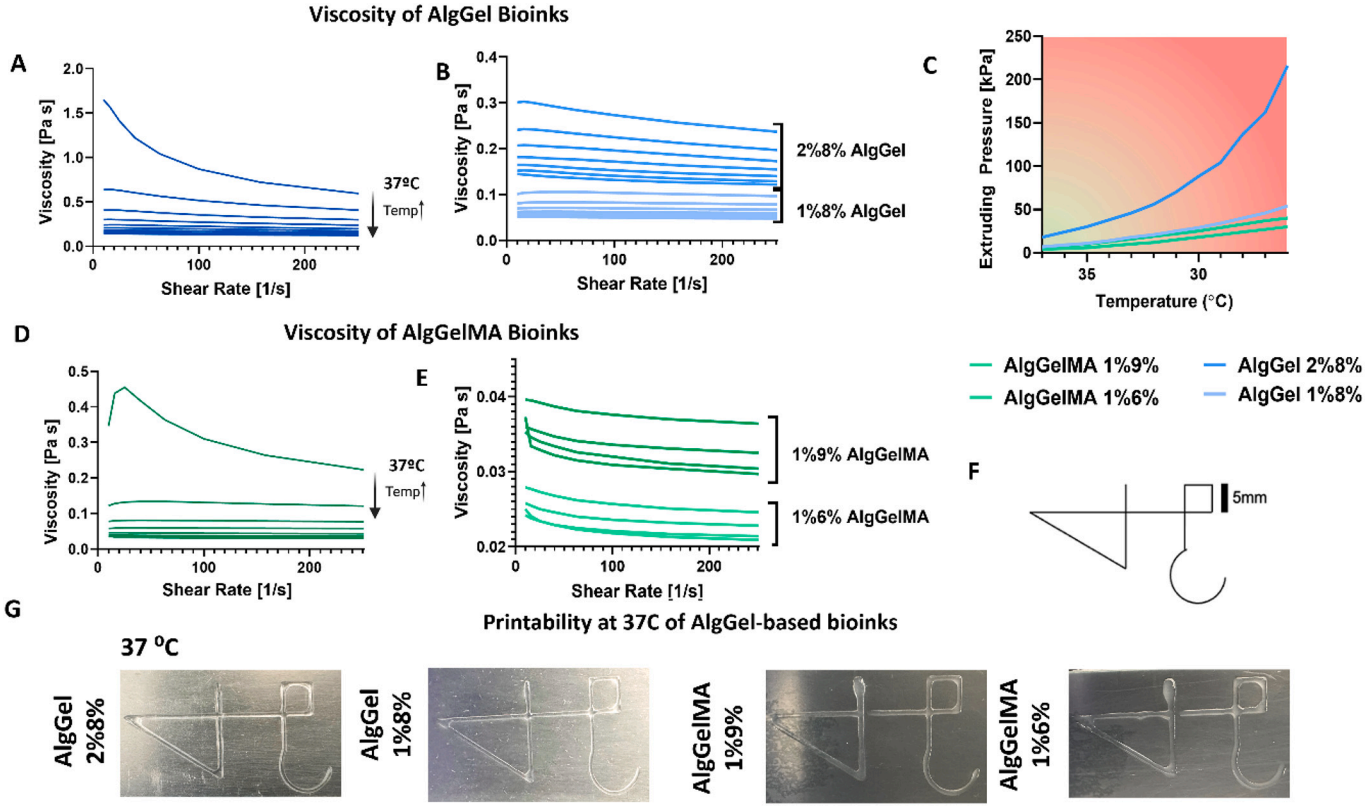

Fig. 2. Viscosity and printability of AlgGel- and AlgGelMA-based bioinks. Viscosities of AlgGel and AlgGelMA bioinks were measured by rheometry using a conical plate of 60 mm. The surface of the rheometer was allowed to warm to 37 °C before the first curve was measured. 3 mL of hydrogel solution was loaded. AlgGel 2 %8 % viscosity (A) is compared to AlgGel 1 %8 % in (B). Displayed temperature ranges are 37–30 °C (lowest to highest curve) for A, and 37–31 °C for B. Extruding pressure required at different temperatures (C). AlgGelMA 1 %9 % viscosity (D) is compared to AlgGelMA 1 %6 % viscosity in (E). Displayed temperature ranges are 37–25 °C for (D), and 37–26 °C for (E). Printability assessment constructs printed at 37 °C for all bioinks (G) following pre-designed model (F).

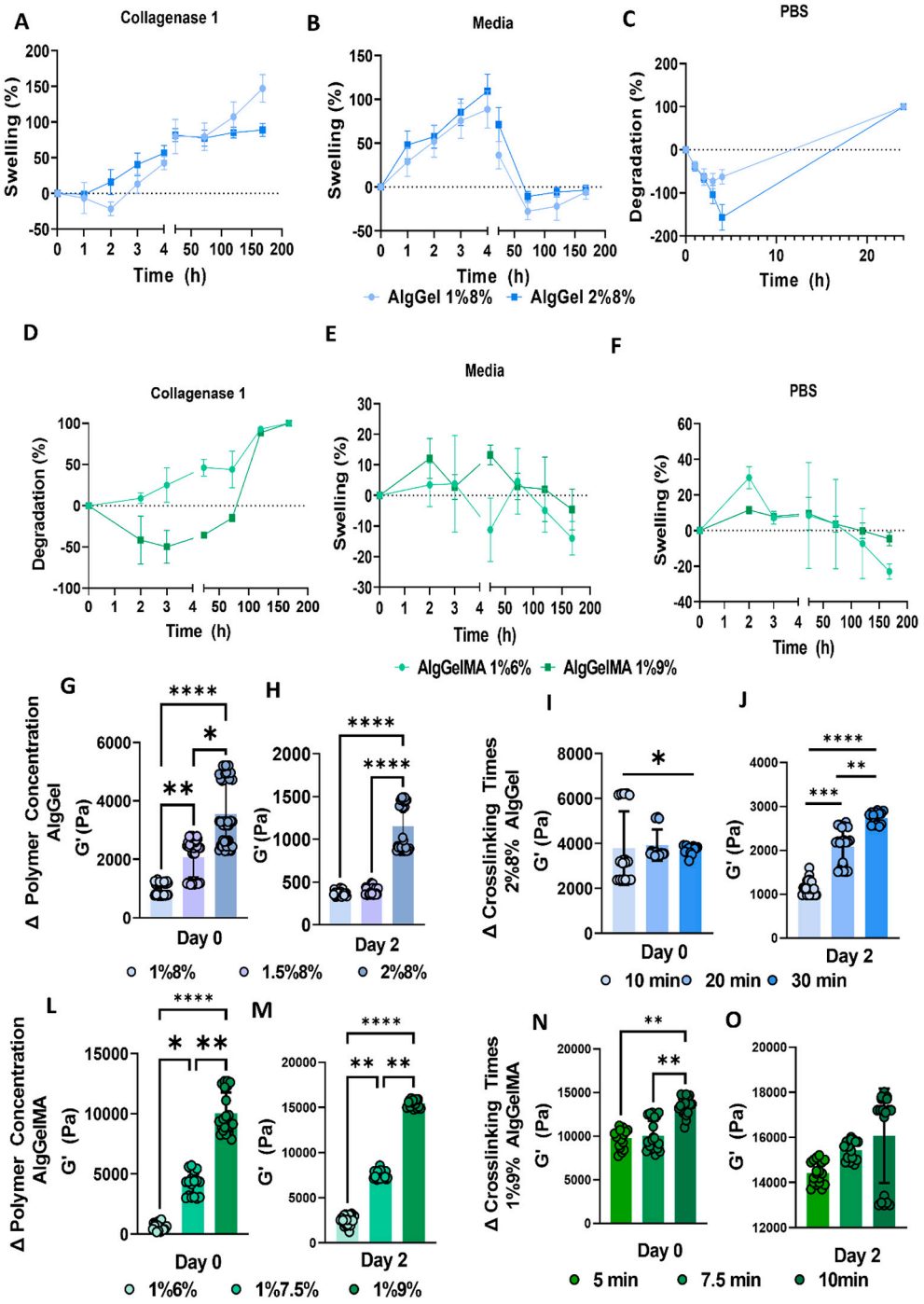

Fig. 3. AlgGel-based bioinks exhibit different physicochemical properties. Degradation and Swelling of AlgGel/GelMA using different solutions displaying weight lost with respect to initial weight (degradation) and weight increase with respect to initial weight (Swelling) (A-F). Storage Modulus (Pa) for different AlgGel formulations at day 0 (G) and day 2 (H). Storage Modulus (Pa) for a 2 %8 % AlgGel bioink using various crosslinking times at day 0 (I) and day 2 (J). Storage Modulus (Pa) for different AlgGelMA formulations at day 0 (L) and day 2 (M). Storage Modulus (Pa) for a 1 %9 % AlgGelMA bioink, crosslinking for different times at day 0 (N) and day 2 (O).

crosslinking times resulted in AlgGel2%8 % hydrogels with a less pronounced decrease in storage modulus (Fig. 3J). Overall, this data reflects the tuneable stiffness of these gels, with Young's moduli – usually defined as the stiffness of a substance [55] – ranging from 3 to 9 kPa.

The storage modulus of AlgGelMA hydrogel families did not decrease after two days in cell culture conditions, indicating that these conditions do not significantly reduce the stability of the gel network (Fig. 3L & M). Additionally, an increase in storage modulus with higher GelMA concentrations was observed. This concurs with previous studies using GelMA hydrogels, which found that hydrogel networks comprising of higher GelMA concentrations had a thicker fibre width, which could contribute to the greater storage modulus (Y. [56]). Increasing the crosslinking time resulted in a higher initial storage modulus when.

crosslinked for 10 min compared to 5 and 7.5 min, however, after two days no significant differences were found (Fig. 3N & O). Similar to AlgGel hydrogels, the stiffness of these gels is controllable, with a wide range of Young's moduli of approximately 6–40 kPa. This flexibility enables the replication of a wide array of tissue properties.

It has been widely documented that the mechanical properties of hydrogels, such as stiffness, can direct cell behaviour and fate ([57–61]). Stiffness has been used to direct biological responses, showing that substrate stiffness alone can lead to differences in cell spreading or promote stem cell differentiation in gels [62]. In this work, we produced hydrogels with controlled Young's modulus ranging from 1.5 to 4.5 kPa for AlgGel bioinks, and ranging from 6 kPa to over 40 kPa in AlgGelMA bioinks. This range of stiffness control, based on polymer concentration, provides a platform that is not only printable, but also able to recapitulate a wide range of mechanical properties present in native tissues (Fig. 3G – O) such as brain (2–3 kPa ([63]; C. [64])), liver (4–6 kPa [65,66] and heart (5–50 kPa [55,67]).

3.6. Microarchitecture of AlgGel and AlgGelMA hydrogels

In order to model the *in vivo* environment, the hydrogel microarchitecture, such as pore size, porosity and fibre diameter, must closely emulate the native tissue ECM [68,69]. The hydrogel microarchitecture can affect flow of materials through the hydrogel, cell behaviour, and proliferation [68–70]. For example, an elegant study by Bova et al. compared GelMA hydrogels alone to GelMA blended with Pluronic, and they found a higher level of cell viability and organisation within the more porous GelMA-Pluronic hydrogels compared to GelMA, which was relatively less porous [71]. As there was minimal difference in Young's Modulus between the blends, they hypothesised that the differences in microarchitecture influenced the cell behaviour and viability. Here, scanning electron microscopy (SEM) and microcomputed tomography (μCT) were used to investigate the microarchitecture of AlgGel and AlgGelMA bioinks of selected concentrations (Fig. 4).

The data revealed that all bioinks displayed a highly porous structure. Compared to AlgGel 2 %8 % hydrogels, AlgGel 1 %8 % hydrogel structure displayed a six-fold higher average pore area and wider range of pore sizes (8959 ± 8053 μm^2 for AlgGel 1 %8 % hydrogels compared to 1319 ± 981 μm^2 for AlgGel 2 %8 %), reflecting that AlgGel 1 %8 %

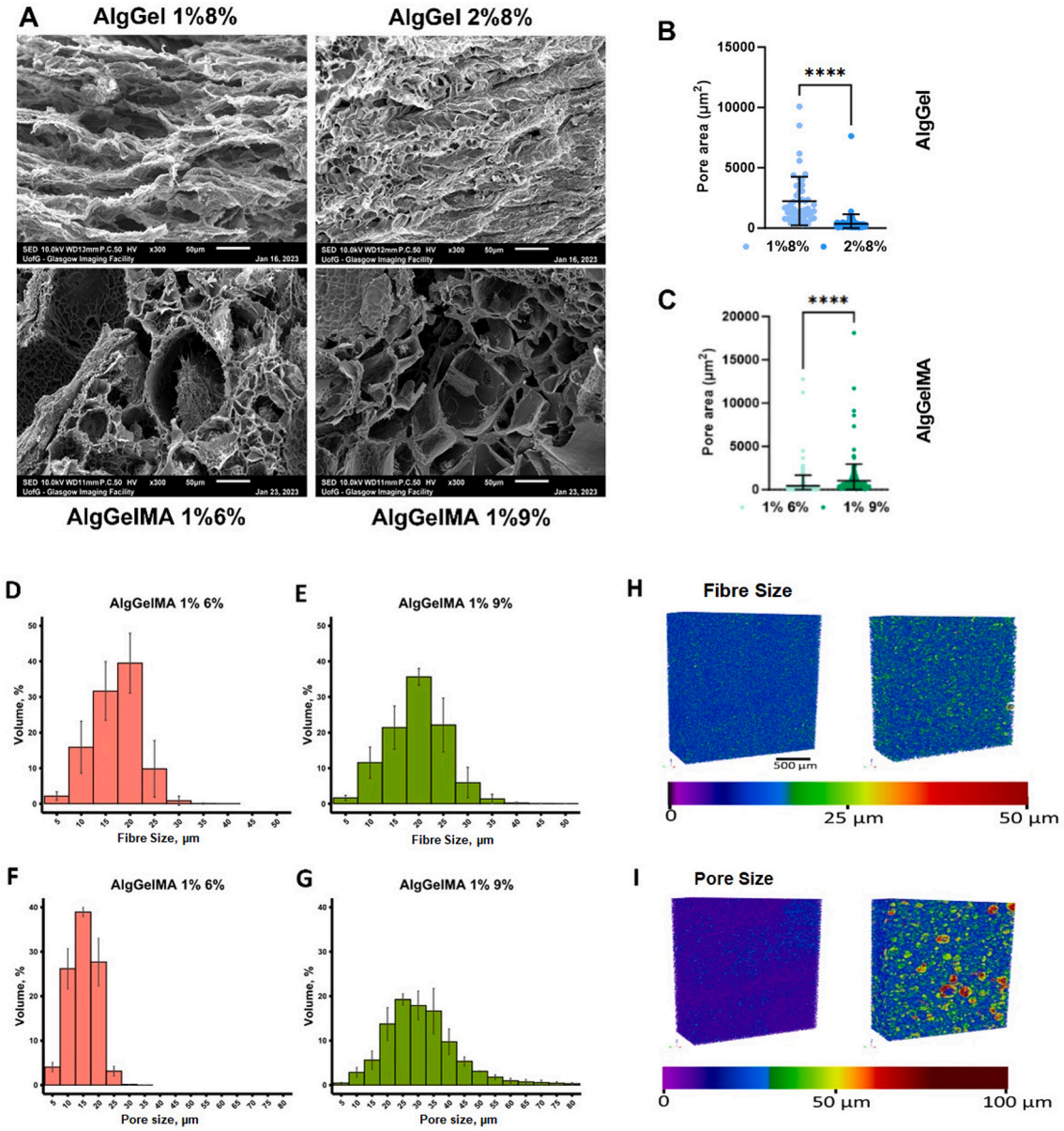

Fig. 4. Representative SEM images of AlgGel/AlgGelMA bioinks after freeze-drying (A). Pore area for AlgGel (B) and AlgGelMA (C) bioinks. Graphs show individual values, mean ± SD; significance assessed using Mann Whitney *U* test. Histograms displaying the polymer density (D, E) and pore size (F, G) of AlgGelMA hydrogels of selected concentrations as elucidated through μCT. Representative images visualising the fibre density (H) and pore size (I) of AlgGelMA 1 %6 % (left) and AlgGelMA 1 %9 %(right) as observed through μCT.

structure was more heterogenous with larger pores (Fig. 4B). This could be explained by the increased alginate concentration in the AlgGel 2 %8 % hydrogels, hence providing more Ca^{2+} crosslinking sites. Previous research has found that increasing the alginate concentration produces hydrogels with smaller pore sizes [72,73]. Our results agree with these findings.

In comparison to the AlgGel hydrogels, the AlgGelMA hydrogels appeared to have higher porosity (Fig. 4C). Additionally, the pore area increased with higher GelMA concentrations (1796 ± 4892 μm^2 for AlgGelMA 1 %6 % compared to 4150 ± 8594 μm^2 for AlgGelMA 1 %9 % hydrogels in SEM; through μCT the median pore size was 15 μm and 25 μm respectively), in contrast to previous work where an increase in GelMA concentration resulted in an equal if not smaller pore size (Y. [74]). Nonetheless, it is important to consider the presence of alginate, which might interact with the GelMA network, in a similar way to particle incorporation in hydrogels [75]. Additionally, previous research whereby other polymers have been incorporated into GelMA networks have resulted in increased pore size with increasing GelMA concentrations [56]. The presence of additional components could disrupt the GelMA network, resulting in a larger pore size.

However, considering equal volume of the freeze-dried sample, concentration should lead to a measurably higher quantity of material in the network (considering it has not left the final construct). Despite not being able to quantify this *via* SEM, μCT analysis for AlgGelMA samples show increased fibre thickness with increasing concentrations of GelMA, which could explain how the polymer has arranged within the network (forming thicker fibres).

3.7. AlgGel and AlgGelMA bioinks provide different cell instructive properties for different cell types and spheroids

Viability of human Mesenchymal Stem Cells (hMSCs) after printing was measured to evaluate the cytocompatibility of the bioinks and any toxicity associated with the printing process. As higher polymer concentrations have been linked to lower cell viability, we performed the experiment only with the highest concentration polymer for each bioink family [76]. Further, 8 % Gel and 9 % GelMA displayed similar printability, hence were selected for further experiments.

hMSC Viability was measured within both AlgGel and AlgGelMA bioinks after printing. Here, similar trends and values were observed compared to bulk hydrogels, with viability ranging between 70 and 80 % (supplementary fig. 3). AlgGel bioinks showed an initial decrease in viability that was recovered by day 7 (supplementary fig. 3). However, it must be noted that cells bioprinted in AlgGel bioinks remain rounded and showed no sign of cell spreading for the duration of the experiment. Contrarily, hMSCs encapsulated within AlgGelMA bioinks adopted more elongated morphologies (supplementary fig. 3). Together, this could indicate that hMSCs remain rounded within hydrogels where alginate is the crosslinking polymer as alginate lacks cell adhesive sites and MMP-cleavable sites. This prevents the cells from binding to and remodelling their surroundings, and therefore spreading. Roundness of cells used in AlgGel bioink is a trait that has been observed previously by other groups [77]. Conversely, AlgGelMA hydrogels contain gelatine as the crosslinking polymer within the gel, which contains many cell binding motifs and MMP-degradable sites, allowing the hMSCs to bind to and degrade the gel matrix, and hence spread throughout the matrix. This concurs with results observed in current literature, which has found hMSC spreading when cultured within GelMA-based hydrogels [78,79].

The biological properties of both AlgGel and AlgGelMA bioink families were tested with different types of cells and spheroids. Cell-adhesive features as well as physicochemical properties can lead to highly different biological responses. For example, adhesion ligands can be included or excluded to control biological processes like stemness [32] or quiescence [33]. Further, to accurately mimic biological systems, mechanical properties must be considered. For instance, the bone marrow provides a softer environment, while cortical bone exhibits significantly higher stiffness and strength [37]. Therefore, cells must be cultured within *in vitro* environments of a similar stiffness compared to their *in vivo* environment.

Different cell types (adherent and non-adherent) and multicellular systems *i.e.*, spheroids were used to study the cell-instructive properties and highlight the importance of cell adhesion domains and physicochemical properties of AlgGel and AlgGelMA bioinks. To visualise morphological changes, actin staining was carried out on printed constructs containing either cell type/conformation (Figs. 5–7).

3.8. Human monocytes (THP-1)

To evaluate the ability of both bioink families to support suspension cells, an Acute Monocytic Leukaemia cell line, THP-1, was used. THP-1 cells are often selected due to their potential to differentiate into mature myeloid cells such as macrophages. Whilst monocytes derived from primary patient samples could be preferable, they are limited in number, can display reduced viability after storage in liquid nitrogen, and require a cocktail of factors to prevent apoptosis [80]. Therefore, THP-1 cells have been widely used and accepted as a model to study modulation of monocyte and macrophage activities.

THP-1 cells cultured in 4.5 kPa AlgGel 2 %8 % bioprinted constructs formed clusters, with cluster size, number of cells per cluster, and aspect ratio of the cluster increasing with time (Fig. 5A-D). Clustering of undifferentiated THP-1 cells has been displayed previously in 3D *in vitro* systems [81], a feature that could be connected to increased leukemic potential [82]. However, the small pore size of AlgGel 2 %8 % hydrogels may impede the migration of THP-1 cells, resulting in clusters as cells cannot migrate following proliferation. However, the area of THP-1 cells (Fig. 1D) would indicate that in earlier timepoints they are small enough to fit within the pores, so additional factors must prevent them from doing so. Hence, the clustering could be due to the absence of cell binding motifs and MMP-cleavable sites in the AlgGel network. The THP-1 cells may not be able to degrade the gel, therefore the cluster size may increase as the new cells that are produced during cell division are unable to migrate for this reason.

When cultured in AlgGelMA 1 %9 % hydrogels, which exhibit a stiffness of approximately 40 kPa, THP-1 cells followed a similar trend, however, the number of cells per cluster was lower and the average cluster size was smaller (Fig. 5E-H). AlgGelMA hydrogels contain MMP-cleavable sites within the crosslinking polymer (GelMA), therefore cells can degrade these sites in order to remodel their environment. GelMA also contains cell binding motifs to enable interaction between the cells and their environment. For these reasons, THP-1 cells within AlgGelMA hydrogels may be able to migrate through the gel, resulting in smaller clusters. Additionally, the pore size of AlgGelMA 1 %9 % hydrogels is larger than those of AlgGel 2 %8 % hydrogels, which could further promote THP-1 cell migration through the gel. Migration of suspension cells, including THP-1, through GelMA-based hydrogels has previously been observed (J. [83,84]). Overall, these data reflect that both AlgGel and AlgGelMA are capable of supporting suspension cells, such as THP-1 cells, for up to seven days in culture.

3.9. Human mesenchymal stem cells

To evaluate the response of adherent cells, hMSCs were selected as they have previously been used to model cell behaviours including differentiation, migration and spreading [83,85,86]. hMSCs are multipotent cells, with the ability to self-renew and differentiate into multiple cell types, including osteoblasts and adipocytes, making them key players in tissue healing and regeneration [62,87].

Previous studies have used these cells to identify the differentiation of stem cells in different scenarios. For example, they have been used to study processes such as osteogenesis, where these cells acquire essential roles in the bone formation or remodelling processes [88]. Moreover, hMSC are the most transplanted cell type, which underscores why the

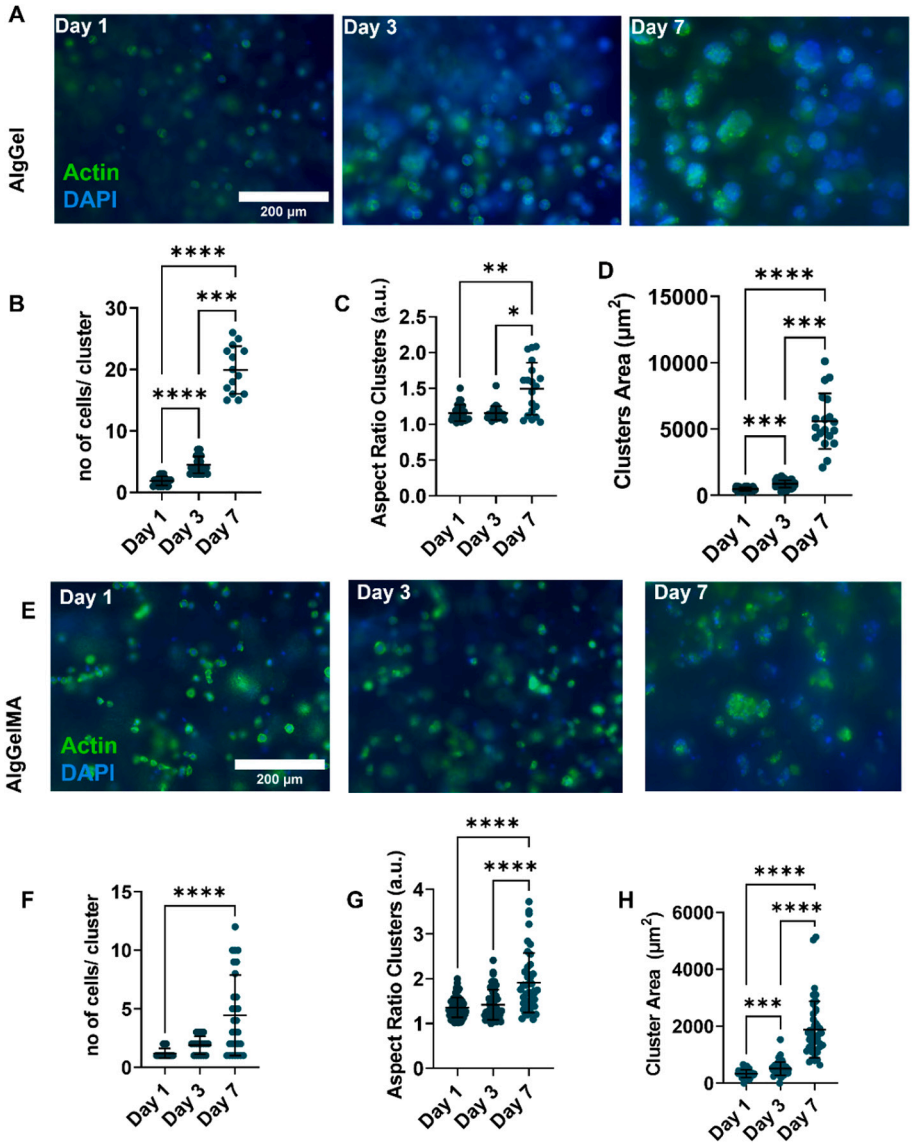

Fig. 5. THP-1 response within bioprinted AlgGel-based bioinks. Representative images are shown in (A) for AlgGel 2 %8 % on day 1 (left), day 3 (mid), and day 7 (right). The number of clusters, aspect ratio of the clusters, and cluster area are shown in (B), (C) and (D). Representative images are shown in (E) for AlgGelMA 1 %9 % at day 1 (left), day 3 (mid) and day 7 (right). The number of clusters, aspect ratio of the clusters and cluster area are shown in (F), (G) and (H). Graphs are shown as individual values ± SD. Significant differences were analysed by the Kruskal-Wallis test.

maintenance of hMSC populations in a stem-like state or a metabolically inactive state, for purposes such as hMSC storage or transport, is an increasingly popular area in current research [89,90]. Previous studies have tried to mitigate unwanted stem cell differentiation both by using both chemical and physical factors [91] and by generating stem cell spheroids, which will be explored below [92].

In this work, when hMSCs were cultured in the 4.5 kPa (AlgGel) bioinks, cells showed no sign of morphological change, staying round over time (Fig. 6A–D). The stemness of hMSCs [93], and other metabolically inactivated states, have been linked to rounder cell morphologies [94]. Morphological changes are often linked with decreasing differentiation potential, whereas round and smaller morphologies are associated with more stem-like phenotypes [93,95]. Similarly, when differentiation occurs, round morphologies have been associated with adipogenic and chondrogenic differentiation, while more spread morphologies with myogenic or osteogenic differentiation. Despite these indications, no clear assumption can be made regarding their stemness or differentiation purely based on their morphology.

Contrarily, when hMSCs were encapsulated in 40 kPa adherent (AlgGelMA) bioinks, cells showed clear morphological changes (Fig. 6). All shape descriptors revealed bigger, more spread cell morphologies, previously associated with osteogenic differentiation, in a time-dependent manner (Fig. 6E-H). These results concur with previous research, where hMSC spreading was observed within hydrogels containing MMP-cleavable sites, including GelMA-based hydrogels [79,96,97]. However, a contributing factor toward the spread of hMSCs within the gel within AlgGelMA could be that the pore size is larger than that of AlgGel 2 %8 %, enabling the cells to migrate through. Overall, these results highlight how selectively polymer crosslinking, hence modulating physicochemical properties in printable hydrogels provides a versatile platform to study different, but relevant, scenarios within the same cell type.

3.10. *Human mesenchymal stem cell spheroids*

When cultured in conditions that prevent adhesion to a surface, some adherent cells, such as hMSCs, can self-assemble to form 3D cellular aggregates known as spheroids. They have been widely used as they

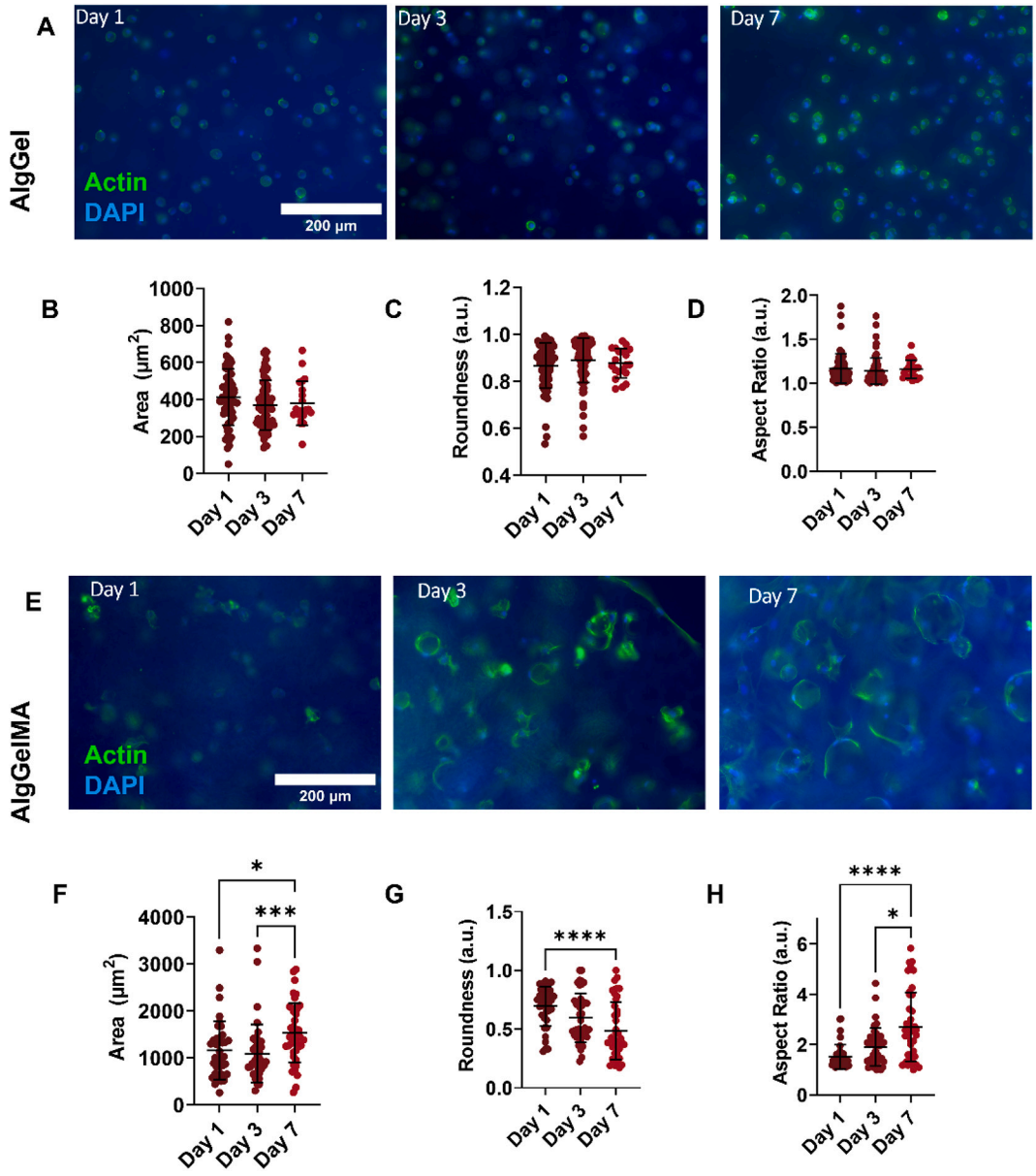

Fig. 6. hMSC response within bioprinted AlgGel-based bioinks. Representative images are shown in (A) for AlgGel 2 % 8 % at day 1 (left), day 3 (mid) and day 7 (right). Area, Roundness and Aspect Ratio are shown in (B), (C) and (D). Representative images are shown in (E) for AlgGelMA 1 % 9 % at day 1 (left), day 3 (mid) and day 7 (right). Area, Roundness and Aspect Ratio are shown in (F), (G) and (H). Graphs are shown as individual values ± SD. Significant differences were analysed using the Kruskal-Wallis test.

provide an environment closer to *in vivo* conditions compared to traditional 2D monolayers, facilitating the presence of cell-cell and cell-matrix interactions. The methods to form them include hanging drop, gel embedding, magnetic levitation, spinner culture, and culturing in low-adherence plates [98–100]. Most adherent cells can form spheroids, and more than one cell type can be present in the spheroid [101].

hMSC spheroids have been shown to have increased viability and increased secretion of cytokines such as Vascular Endothelial Growth Factor (VEGF) and IL-8 compared to single hMSCs [102]. However, their use in clinical applications like cell therapies requires the expansion of a high number of undifferentiated hMSCs. Spheroids can be used to maintain stem-like hMSCs, as cells within hMSC spheroids display increased stemness and retain their self-renewal capabilities, where typically spheroids can be seen keeping their round morphology [92,103]. Also, spheroids retained the conformation and show higher expression of stemness markers, like nestin and STRO-1 [92]. Similarly, cells in spheroid conformations have shown not only upregulation of stemness markers in both hMSC and cancer spheroids [104,105], but also delayed replicative senescence compared to cells cultured in 2D [106]. These morphologic characteristics were observed in this work when using AlgGel bioinks. In fact, spheroids retained their conformation for up to 7 days in culture, possibly indicating a more stem-like phenotype (Fig. 7A–D).

Stem cell spheroids have also been used in tumour models, where they display chemotherapeutic resistance and biochemical responses similar to parental tumours [107]. Moreover, previous work engineered a cancer microenvironment in which cells migrated out of the spheroids and invaded the hydrogel matrix, reproducing a more metastatic phenotype [108]. These phenotypic changes were captured in this work too when using AlgGelMA bioinks, where hMSCs could be seen leaving the spheroids and invading the matrix (Fig. 7E-H). The GelMA matrix, unlike AlgGel, is comprised of cell binding and MMP cleavable sites, which enables cells embedded within to interact with the matrix, allowing cell spreading and migration. This, coupled with the large pore

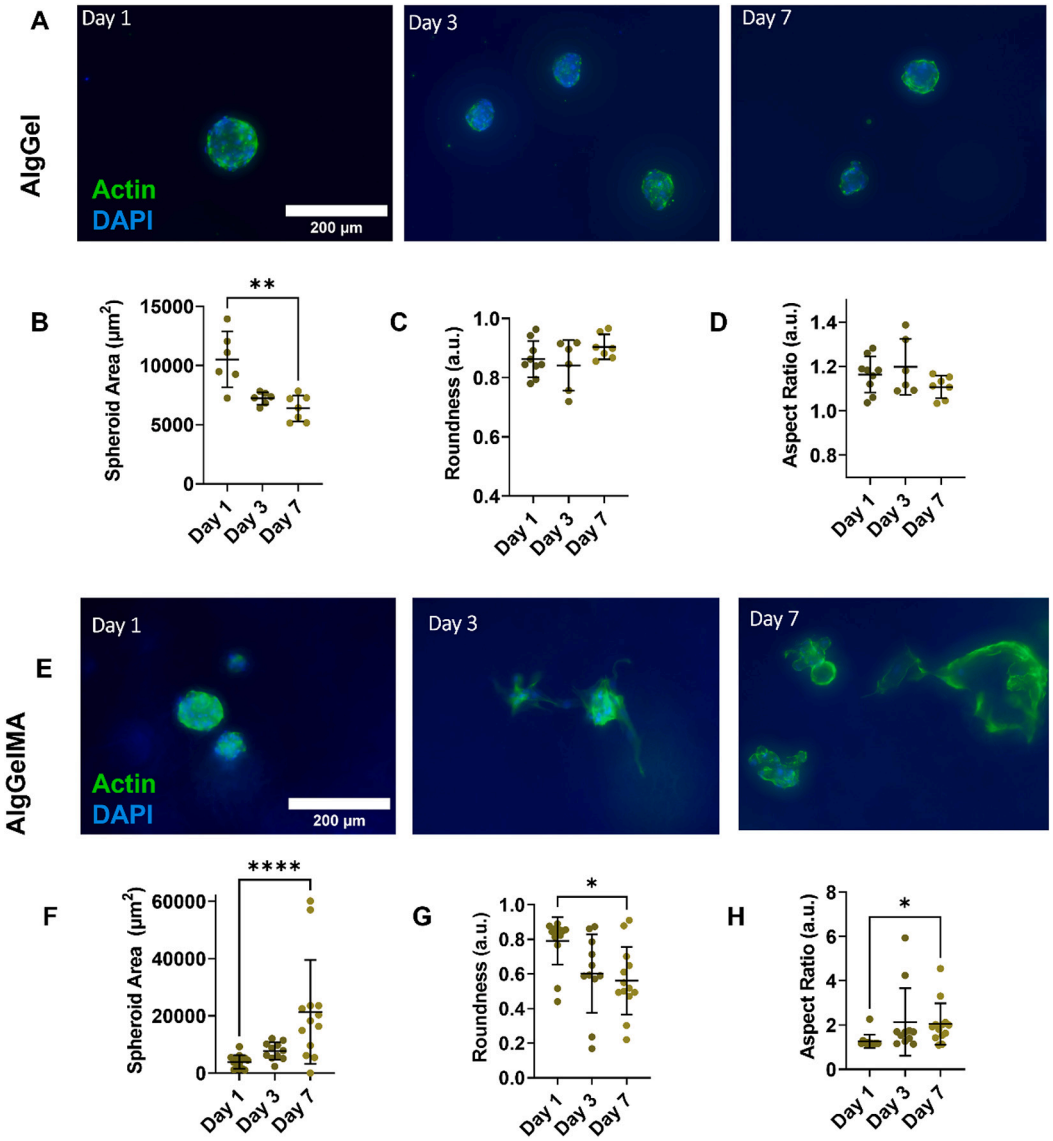

Fig. 7. hMSC Spheroid response bioprinted in AlgGel-based bioinks. Representative images are shown in (A) for AlgGel 2 %8 % at day 1 (left), day 3 (mid) and day 7 (right). Spheroid area, Roundness and Aspect Ratio are shown in (B), (C) and (D). Representative images are shown in (E) for AlgGelMA 1 %9 % at day 1 (left), day 3 (mid) and day 7 (right). Spheroid area, Roundness and Aspect Ratio are shown in (F), (G) and (H). Graphs are shown as individual values ± SD. Significant differences were analysed by Kruskal-Wallis test.

size present within the AlgGelMA structure, allows cells such as hMSCs to migrate through the network.

3.11. *Effect of cell-adhesion ligands incorporation in AlgGel bioink*

Previous experiments showed differences in hMSC morphologies when cultured within AlgGel and AlgGelMA bioinks were used (Fig. 7). We hypothesised that AlgGel bioinks, contrary to AlgGelMA bioinks, did not possess adhesion ligands, either due to gelatine leaking during crosslinking into the network (gelatine release from gels can be seen in Supplementary fig. 4), or because gelatine is not bioavailable. To study the morphology of hMSCs in a AlgGel bioink known to incorporate bioavailable cell binding motifs, a condition containing RGD-modified alginate was included, and used to fabricate RGD-modified alginate/gelatin (AlgRGDGel) constructs both in 2D and 3D. In this way, we could better understand whether the observed biological responses were limited to the availability of adhesion ligands.

Fig. 8A-D shows the results of a 2D cell adhesion experiment. hMSCs showed an inability to attach to the unmodified AlgGel hydrogel while being able to bind both AlgRGDGel and AlgGelMA hydrogels. This proved that the lack of bioavailability or presence of adhesive ligands in AlgGel could be because the gelatine was not crosslinked. In fact, considering the similar stiffness shown by both AlgGel/AlgRGDGel 2 % 8 % and the AlgGelMA 1 %6 %, it can be seen how only when the adhesive ligands are present in the crosslinked network (AlgRGDGel and AlgGelMA), cells are able to attach and spread. Therefore, this highlights why crosslinking gelatine in AlgGel-based bioinks can lead to different biological properties.

Despite these findings, when we evaluated the effect these cell-adhesion motifs had in 3D (Fig. 8E-H), by using AlgRGDGel bioinks, we observed that cells were not able to spread within both AlgGel and AlgRGDGel conditions. This could be because the AlgRGDGel matrix contains the cell binding site RGD but does not contain MMP-cleavable sites. Thus, the cells can bind to the surface and spread in 2D, but this is inhibited in 3D as the AlgRGDGel matrix cannot be degraded by the cells. On the other hand, hMSCs were able to spread in both AlgGelMA bioinks, where a stiffness-dependent increase in morphological parameters could be seen, with cells in higher stiffness samples displaying

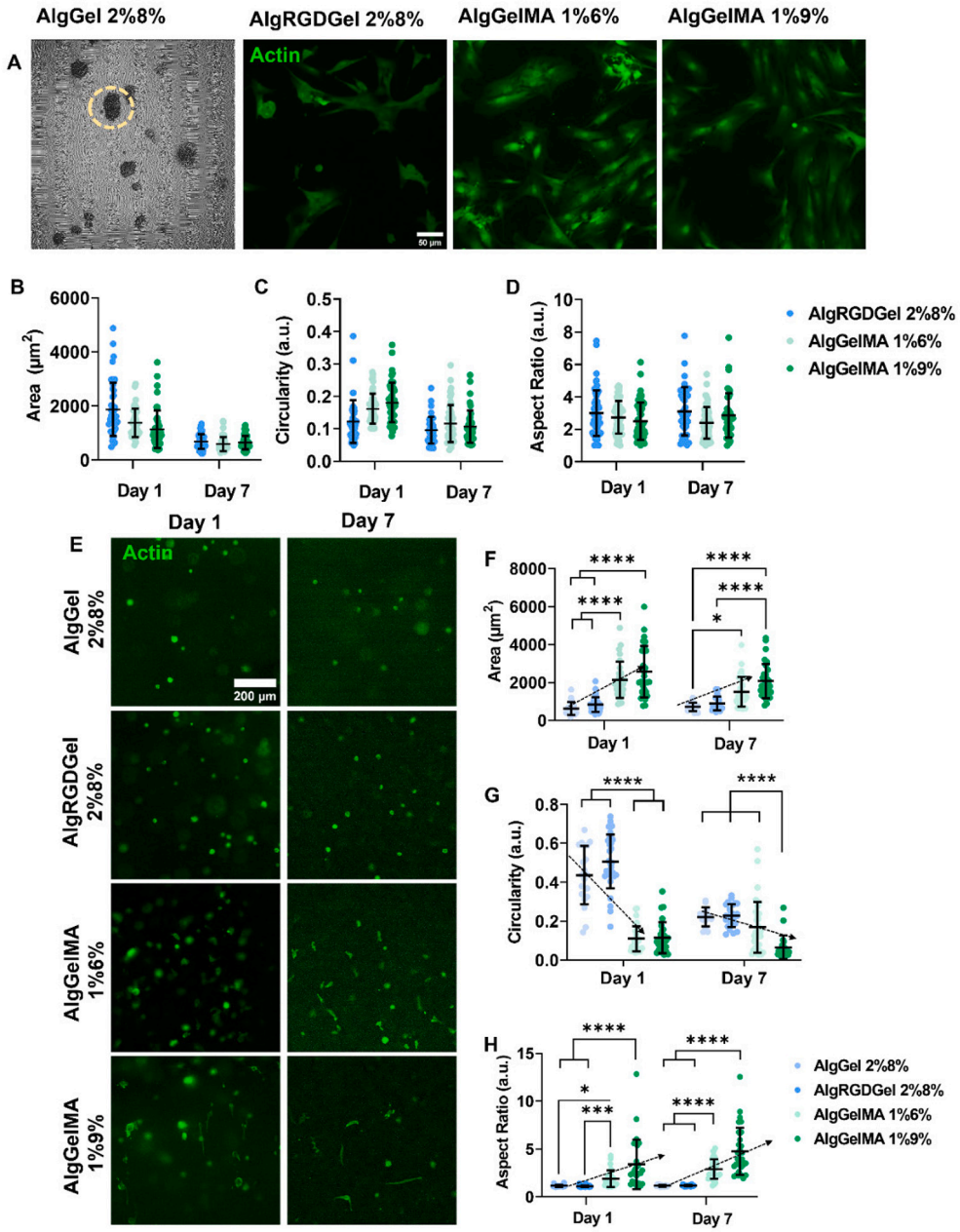

Fig. 8. hMSC response in AlgGel-based bioinks. Representative 2D cell adhesion Day 7 images are shown in (A). Brightfield is shown for AlgGel as cells would detach during staining, Immunofluorescence images depicting Actin are shown for the other conditions. Area, Circularity and Aspect Ratio are shown in (B), (C) and (D). Representative 3D culture cell morphology Day 1 and Day 7 are shown in (E). Area, Circularity and Aspect Ratio are shown in (F), (G) and (H).

larger, more elongated morphologies. Therefore, the presence of a gel network containing cell binding motifs and MMP-degradable sites appears to be the contributing factor which enables cell migration within AlgGelMA hydrogels but not AlgGel hydrogels, rather than differences in pore size.

These data also suggest that the presence of adhesion ligands alone is not driving the morphological changes observed in all cellular models. In fact, both mechanical and degradability properties were seen to be different for both bioink families and have been studied as driving factors in spreading or migration [1,109]. In particular, the stiffness measured for AlgGel bioinks is considerably lower (3–10.7 kPa at day 0; approximately 1.5–4.5 kPa at day2) than those of AlgGelMA bioinks (1.5–30 kPa at day 0; approximately 6–40 kPa at day 2) and might have a great influence on the overall biological response. Nonetheless, the ability of cells to degrade and remodel the matrix surrounding them could be playing an important role. It has been previously shown that alginate-based hydrogels which contain MMP-cleavable sites promote cell spreading in 3D, while presence of cell-binding sites alone does not [1,109].

4. Conclusions

In this present study, the mechanical properties, printability and cell-supportive capabilities of AlgGel and AlgGelMA bioinks were assessed. Both bioinks displayed good printability, with the possibility of bioprinting simple and complex structures. Additionally, through SEM and µCt it was observed that both bioinks had highly porous structures, which further emulate native tissue. AlgGel hydrogels displayed a lower stiffness range whilst AlgGelMA hydrogels were overall stiffer, highlighting that AlgGel may be more suitable for modelling softer tissue

such as bone marrow, and AlgGelMA may be more suitable for modelling of stiffer tissue such as cardiac tissue. Further, both bioinks supported the growth of hMSCs and THP-1 cells for up to seven days in culture. hMSCs were unable to spread and migrate through the AlgGel bioinks, which resulted in rounded morphology of hMSCs and the maintenance of hMSC spheroid shape in culture for the entire seven days. Here, it was postulated that this is due to the lack of MMP cleavable sites within the alginate polymer and lack of cell adhesion sites. This was further confirmed as MSCs were able to spread on top of AlgRGDGel hydrogels but not when encapsulated within these hydrogels. In contrast, MSCs were able to spread within AlgGelMA bioinks, and disruption of spheroid morphology was observed over the course of the experiment. This could be due to the cell binding motifs and MMP-degradable sites within AlgGelMA, facilitating cell migration through the hydrogel matrix. Together, these data highlight that both bioinks are suitable for use in biomimetic *in vitro* models, however, depending on the purpose of the model one may show benefits over the other. For instance, for modelling cell migration AlgGelMA would be superior, whereas for maintaining spheroids within culture AlgGel would be more suitable.

CRediT authorship contribution statement

Alvaro Sanchez-Rubio: Writing – original draft, Methodology, Investigation, Data curation, Conceptualization. **Lauren Hope:** Writing – original draft, Methodology, Investigation. **Eva Barcelona-Estaje:** Writing – review & editing, Investigation. **Vineetha Jayawarna:** Methodology, Investigation. **Jonathan Williams:** Methodology, Investigation. **Manuel Salmeron-Sanchez:** Writing – review & editing, Supervision, Methodology, Investigation, Funding acquisition, Conceptualization.

Declaration of competing interest

Manuel Salmeron Sanchez reports financial support was provided by European Research Council. Manuel Salmeron-Sanchez reports financial support was provided by Engineering and Physical Sciences Research Council. If there are other authors, they declare that they have no known competing financial interests or personal relationships that could have appeared to influence the work reported in this paper.

Acknowledgments

We acknowledge financial support from the European Research Council AdG (Devise, 101054728 to M.S..S) and EPSRC HT2050 grant (EP/X033554/1 to M.S.S) L.H and A,S,R were funded by the LIFETIME CDT and Medical Research Scotland (PhD 1175-2017) respectively. IBEC is a recipient of a Severo Ochoa Award of Excellence from MINCIN and member of CERCA Programme/Generalitat de Catalunya.

Appendix A. Supplementary data

Supplementary data to this article can be found online at https://doi.org/10.1016/j.bioadv.2025.214408.

Data availability

Data will be made available on request.

References

[1] K.B. Fonseca, D.B. Gomes, K. Lee, S.G. Santos, A. Sousa, E.A. Silva, D.J. Mooney, P.L. Granja, C.C. Barrias, Injectable MMP-sensitive alginate hydrogels as hMSC delivery systems, Biomacromolecules 15 (1) (2014) 380–390, https://doi.org/10.1021/bm4016495.

[2] Z. Li, K.M. Bratlie, Effect of RGD functionalization and stiffness of gellan gum hydrogels on macrophage polarization and function, Materials Science and Engineering C 128 (2021), https://doi.org/10.1016/j.msec.2021.112303.

[3] S. Ansari, S. Pouraghaei Sevari, C. Chen, P. Sarrion, A. Moshaverinia, RGD-modified alginate-GelMA hydrogel sheet containing gingival mesenchymal stem cells: a unique platform for wound healing and soft tissue regeneration, ACS Biomaterials Science and Engineering 7 (8) (2021) 3774–3782, https://doi.org/10.1021/acsbiomaterials.0c01571.

[4] S. Ansari, P. Sarrion, M.M. Hasani-Sadrabadi, T. Aghaloo, B.M. Wu, A. Moshaverinia, Regulation of the fate of dental-derived mesenchymal stem cells using engineered alginate-GelMA hydrogels, Journal of Biomedical Materials Research - Part A 105 (11) (2017) 2957–2967, https://doi.org/10.1002/jbm.a.36148.

[5] H. Ding, N.P. Illsley, R.C. Chang, 3D bioprinted GelMA based models for the study of trophoblast cell invasion, Sci. Rep. 9 (1) (2019), https://doi.org/10.1038/s41598-019-55052-7.

[6] A. Micalet, E. Moeendarbary, U. Cheema, 3D in vitro models for investigating the role of stiffness in cancer invasion, ACS Biomater. Sci. Eng. (2021), https://doi.org/10.1021/acsbiomaterials.0c01530.

[7] A. Sanchez-Rubio, V. Jayawarna, E. Maxwell, M.J. Dalby, M. Salmeron-Sanchez, Keeping it organized: multicompartment constructs to mimic tissue heterogeneity, Adv. Healthc. Mater. (2023), https://doi.org/10.1002/adhm.202202110.

[8] Ž.P. Kačarević, P.M. Rider, S. Alkildani, S. Retnasingh, R. Smeets, O. Jung, Z. Ivanišević, M. Barbeck, An introduction to 3D bioprinting: possibilities, challenges and future aspects, Materials 11 (11) (2018), https://doi.org/10.3390/ma11112199.

[9] Murphy, S. V., & Atala, A. (2014). 3D bioprinting of tissues and organs. In Nature Biotechnology (Vol. 32, Issue 8, pp. 773–785). Nature Publishing Group. doi:https://doi.org/10.1038/nbt.2958.

[10] Y. Baert, K. Dvorakova-Hortova, H. Margaryan, E. Goossens, Mouse in vitro spermatogenesis on alginate-based 3D bioprinted scaffolds, Biofabrication 11 (3) (2019), https://doi.org/10.1088/1758-5090/ab1452.

[11] J. Hauptstein, L. Forster, A. Nadernezhad, J. Groll, J. Teßmar, T. Blunk, Tethered TGF-β1 in a hyaluronic acid-based bioink for bioprinting cartilaginous tissues, Int. J. Mol. Sci. 23 (2) (2022), https://doi.org/10.3390/ijms23020924.

[12] Z. Li, S. Huang, Y. Liu, B. Yao, T. Hu, H. Shi, J. Xie, X. Fu, Tuning alginate-gelatin bioink properties by varying solvent and their impact on stem cell behavior, Sci. Rep. 8 (1) (2018) 1–8, https://doi.org/10.1038/s41598-018-26407-3.

[13] J.Y. Park, J.C. Choi, J.H. Shim, J.S. Lee, H. Park, S.W. Kim, J. Doh, D.W. Cho, A comparative study on collagen type i and hyaluronic acid dependent cell behavior for osteochondral tissue bioprinting, Biofabrication 6 (3) (2014), https://doi.org/10.1088/1758-5082/6/3/035004.

[14] S.Y. Sonaye, E.G. Ertugral, C.R. Kothapalli, P. Sikder, Extrusion 3D (bio)printing of alginate-gelatin-based composite scaffolds for skeletal muscle tissue engineering, Materials 15 (22) (2022), https://doi.org/10.3390/ma15227945.

[15] M.H. Kim, C.C. Lin, Poly(ethylene glycol)-norbornene as a photoclick bioink for digital light processing 3D bioprinting, ACS Appl. Mater. Interfaces. (2022), https://doi.org/10.1021/acsami.2c20098.

[16] M. Müller, J. Becher, M. Schnabelrauch, M. Zenobi-Wong, Nanostructured Pluronic hydrogels as bioinks for 3D bioprinting, Biofabrication 7 (3) (2015), https://doi.org/10.1088/1758-5090/7/3/035006.

[17] M.A. Heinrich, R. Bansal, T. Lammers, Y.S. Zhang, R. Michel Schiffelers, J. Prakash, 3D-bioprinted Mini-brain: a glioblastoma model to study cellular interactions and therapeutics, Adv. Mater. 1806590 (2019) 1–9, https://doi.org/10.1002/adma.201806590.

[18] S. Galarza, A.J. Crosby, C.H. Pak, S.R. Peyton, Control of astrocyte quiescence and activation in a synthetic brain hydrogel, Adv. Healthc. Mater. 9 (4) (2020) 1–12, https://doi.org/10.1002/adhm.201901419.

[19] Y. Matsumura, Y. Zhu, H. Jiang, A. D'Amore, S.K. Luketich, V. Charwat, T. Yoshizumi, H. Sato, B. Yang, T. Uchibori, K.E. Healy, W.R. Wagner, Intramyocardial injection of a fully synthetic hydrogel attenuates left ventricular remodeling post myocardial infarction, Biomaterials 217 (June) (2019) 119289, https://doi.org/10.1016/j.biomaterials.2019.119289.

[20] S.O. Sarrigiannidis, J.M. Rey, O. Dobre, C. González-García, M.J. Dalby, M. Salmeron-Sanchez, A tough act to follow: collagen hydrogel modifications to improve mechanical and growth factor loading capabilities, Mater. Today Bio. (2021), https://doi.org/10.1016/j.mtbio.2021.100098.

[21] P.S. Gungor-Ozkerim, I. Inci, Y.S. Zhang, A. Khademhosseini, M.R. Dokmeci, Bioinks for 3D bioprinting: an overview, Biomater. Sci. 6 (5) (2018) 915–946, https://doi.org/10.1039/c7bm00765e.

[22] S.V. Murphy, P. De Coppi, A. Atala, Opportunities and challenges of translational 3D bioprinting, Nat. Biomed. Eng. 4 (4) (2020) 370–380, https://doi.org/10.1038/s41551-019-0471-7.

[23] Schwab A. Levato R. D'Este M. Piluso S. Eglin D. Malda J. 2020 Printability and shape fidelity of bioinks in 3D bioprinting Chem. Rev. 120 19 11028 11055 American Chemical Society https://doi.org/10.1021/acs.chemrev.0c00084.

[24] J.H.Y. Chung, S. Naficy, Z. Yue, R. Kapsa, A. Quigley, S.E. Moulton, G.G. Wallace, Bio-ink properties and printability for extrusion printing living cells, Biomater. Sci. 1 (7) (2013) 763–773, https://doi.org/10.1039/c3bm00012e.

[25] T. Jiang, J.G. Munguia-Lopez, K. Gu, M.M. Bavoux, S. Flores-Torres, J. Kort-Mascort, J. Grant, S. Vijayakumar, A. De Leon-Rodriguez, A.J. Ehrlicher, J. M. Kinsella, Engineering bioprintable alginate/gelatin composite hydrogels with tunable mechanical and cell adhesive properties to modulate tumor spheroid growth kinetics, Biofabrication 12 (1) (2020), https://doi.org/10.1088/1758-5090/ab3a5c.

[26] T. Gao, G.J. Gillispie, J.S. Copus, A.P.R. Kumar, Y.J. Seol, A. Atala, J.J. Yoo, S. J. Lee, Optimization of gelatin-alginate composite bioink printability using rheological parameters: a systematic approach, Biofabrication 10 (3) (2018), https://doi.org/10.1088/1758-5090/aacdc7.
[27] Harrington, W. F., & Von Hippel, P. H. (1962). The structure of collagen and gelatin. Adv. Protein Chem., 16(C), 1–138. https://doi.org/10.1016/S0065-3233(08)60028-5.
[28] Wang X. Ao Q. Tian X. Fan J. Tong H. Hou W. Bai S. 2017 Gelatin-based hydrogels for organ 3D bioprinting Polymers 9 9 MDPI AG https://doi.org/10.3390/polym9090401.
[29] E. Barcelona-Estaje, M.J. Dalby, M. Cantini, M. Salmeron-Sanchez, You talking to me? Cadherin and integrin crosstalk in biomaterial design, Adv. Healthc. Mater. 10 (6) (2021), https://doi.org/10.1002/adhm.202002048.
[30] S.J. Bidarra, C.C. Barrias, K.B. Fonseca, M.A. Barbosa, R.A. Soares, P.L. Granja, Injectable in situ crosslinkable RGD-modified alginate matrix for endothelial cells delivery, Biomaterials 32 (31) (2011) 7897–7904, https://doi.org/10.1016/j.biomaterials.2011.07.013.
[31] N.C. Hunt, D. Hallam, A. Karimi, C.B. Mellough, J. Chen, D.H.W. Steel, M. Lako, 3D culture of human pluripotent stem cells in RGD-alginate hydrogel improves retinal tissue development, Acta Biomater. 49 (2017) 329–343, https://doi.org/10.1016/j.actbio.2016.11.016.
[32] M. Hemadi, V. Assadollahi, G. Saki, A. Pirnia, M. Alasvand, A. Zendehdel, M. Gholami, Use of alginate hydrogel to improve long-term 3D culture of spermatogonial stem cells: stemness gene expression and structural features, Zygote (2021) 1–7, https://doi.org/10.1017/S0967199421000551.
[33] S.A. Ferreira, P.A. Faull, A.J. Seymour, T.T.L. Yu, S. Loaiza, H.W. Auner, A. P. Snijders, E. Gentleman, Neighboring cells override 3D hydrogel matrix cues to drive human MSC quiescence, Biomaterials 176 (2018) 13–23, https://doi.org/10.1016/j.biomaterials.2018.05.032.
[34] A.P.D.N. De Barros, C.M. Takiya, L.R. Garzoni, M.L. Leal-Ferreira, H.S. Dutra, L. B. Chiarini, M.N. Meirelles, R. Borojevic, M.I.D. Rossi, Osteoblasts and bone marrow mesenchymal stromal cells control hematopoietic stem cell migration and proliferation in 3D in vitro model, PloS One 5 (2) (2010), https://doi.org/10.1371/journal.pone.0009093.
[35] L.J. Bray, M. Binner, Y. Körner, M. Von Bonin, M. Bornhäuser, C. Werner, A three-dimensional ex vivo tri-culture model mimics cell-cell interactions between acute myeloid leukemia and the vascular niche, Haematologica 102 (7) (2017) 1215–1226, https://doi.org/10.3324/haematol.2016.157883.
[36] B. Liu, M. Jin, D.A. Wang, In vitro expansion of hematopoietic stem cells in a porous hydrogel-based 3D culture system, Acta Biomater. 161 (2023) 67–79, https://doi.org/10.1016/j.actbio.2023.01.057.
[37] M.R. Nelson, K. Roy, Bone-marrow mimicking biomaterial niches for studying hematopoietic stem and progenitor cells, J. Mater. Chem. B 4 (20) (2016) 3490–3503, https://doi.org/10.1039/c5tb02644j.
[38] R. Li, C. Zhou, J. Chen, H. Luo, R. Li, D. Chen, X. Zou, W. Wang, Synergistic osteogenic and angiogenic effects of KP and QK peptides incorporated with an injectable and self-healing hydrogel for efficient bone regeneration, Bioactive Materials 18 (2022) 267–283, https://doi.org/10.1016/j.bioactmat.2022.02.011.
[39] A. Mondal, A. Gebeyehu, M. Miranda, D. Bahadur, N. Patel, S. Ramakrishnan, A. K. Rishi, M. Singh, Characterization and printability of sodium alginate -gelatin hydrogel for bioprinting NSCLC co-culture, Sci. Rep. 9 (1) (2019), https://doi.org/10.1038/s41598-019-55034-9.
[40] A.I. Van Den Bulcke, B. Bogdanov, N. De Rooze, E.H. Schacht, M. Cornelissen, H. Berghmans, Structural and rheological properties of methacrylamide modified gelatin hydrogels, Biomacromolecules 1 (1) (2000) 31–38, https://doi.org/10.1021/bm990017d.
[41] R. Raman, R. Bashir, Stereolithographic 3D bioprinting for biomedical applications, in: Essentials of 3D Biofabrication and Translation, Elsevier Inc, 2015, pp. 89–121, https://doi.org/10.1016/B978-0-12-800972-7.00006-2.
[42] J. Patten, K. Wang, Fibronectin in development and wound healing, Adv. Drug Deliv. Rev. 170 (2021) 353–368, https://doi.org/10.1016/j.addr.2020.09.005.
[43] S. Suzuki, N. Morimoto, Y. Ikada, Gelatin gel as a carrier of platelet-derived growth factors, J. Biomater. Appl. 28 (4) (2013) 595–606, https://doi.org/10.1177/0885328212468183.
[44] Z. Wei, E. Volkova, M.R. Blatchley, S. Gerecht, Hydrogel vehicles for sequential delivery of protein drugs to promote vascular regeneration, Adv. Drug Deliv. Rev. (2019) 95–106, https://doi.org/10.1016/j.addr.2019.08.005.
[45] G. Gillispie, P. Prim, J. Copus, J. Fisher, A.G. Mikos, J.J. Yoo, A. Atala, S.J. Lee, Assessment methodologies for extrusion-based bioink printability, Biofabrication 12 (2) (2020), https://doi.org/10.1088/1758-5090/ab6f0d.
[46] Y. He, F. Yang, H. Zhao, Q. Gao, B. Xia, J. Fu, Research on the printability of hydrogels in 3D bioprinting, Sci. Rep. 6 (2016), https://doi.org/10.1038/srep29977.
[47] Z. Zhang, Y. Jin, J. Yin, C. Xu, R. Xiong, K. Christensen, B.R. Ringeisen, D. B. Chrisey, Y. Huang, Evaluation of bioink printability for bioprinting applications, Appl. Phys. Rev. 5 (4) (2018), https://doi.org/10.1063/1.5053979.
[48] H.G. Yi, Y.H. Jeong, Y. Kim, Y.J. Choi, H.E. Moon, S.H. Park, K.S. Kang, M. Bae, J. Jang, H. Youn, S.H. Paek, D.W. Cho, A bioprinted human-glioblastoma-on-a-chip for the identification of patient-specific responses to chemoradiotherapy, Nat. Biomed. Eng. 3 (7) (2019) 509–519, https://doi.org/10.1038/s41551-019-0363-x.
[49] H.G. Yi, Y.J. Choi, J.W. Jung, J. Jang, T.H. Song, S. Chae, M. Ahn, T.H. Choi, J. W. Rhie, D.W. Cho, Three-dimensional printing of a patient-specific engineered nasal cartilage for augmentative rhinoplasty, Journal of Tissue Engineering 10 (2019), https://doi.org/10.1177/2041731418824797.
[50] K.A. Homan, D.B. Kolesky, M.A. Skylar-Scott, J. Herrmann, H. Obuobi, A. Moisan, J.A. Lewis, Bioprinting of 3D convoluted renal proximal tubules on Perfusable chips, Sci. Rep. 6 (2016) 34845, https://doi.org/10.1038/srep34845.
[51] F. Maggiotto, L. Bova, S. Micheli, C. Pozzer, P. Fusco, P. Sgarbossa, F. Billi, E. Cimetta, 3D bioprinting for the production of a perfusable vascularized model of a cancer niche, Front. Bioeng. Biotechnol. 13 (2025) 1484738, https://doi.org/10.3389/fbioe.2025.1484738.
[52] K.J. Wolf, J.D. Weiss, S.G.M. Uzel, M.A. Skylar-Scott, J.A. Lewis, Biomanufacturing human tissues via organ building blocks, Cell Stem Cell 29 (5) (2022) 667–677, https://doi.org/10.1016/j.stem.2022.04.012.
[53] K.Y. Lee, D.J. Mooney, Alginate: properties and biomedical applications, Prog. Polym. Sci. 37 (1) (2012) 106–126, https://doi.org/10.1016/j.progpolymsci.2011.06.003.
[54] Piao, Y., You, H., Xu, T., Bei, H. P., Piwko, I. Z., Kwan, Y. Y., & Zhao, X. (2021). Biomedical applications of gelatin methacryloyl hydrogels. In Engineered Regeneration (vol. 2, pp. 47–56). KeAi Communications Co. https://doi.org/10.1016/j.engreg.2021.03.002.
[55] C.F. Guimarães, L. Gasperini, A.P. Marques, R.L. Reis, The stiffness of living tissues and its implications for tissue engineering, Nat. Rev. Mater. 5 (5) (2020) 351–370, https://doi.org/10.1038/s41578-019-0169-1.
[56] Y. Wang, M. Ma, J. Wang, W. Zhang, W. Lu, Y. Gao, B. Zhang, Y. Guo, Development of a photo-crosslinking, biodegradable GelMA/PEGDA hydrogel for guided bone regeneration materials, Materials 11 (8) (2018), https://doi.org/10.3390/ma11081345.
[57] Handorf A. M. Zhou Y. Halanski M. A. Li W. J. 2015 Tissue stiffness dictates development, homeostasis, and disease progression Organogenesis 11 1 1 15 https://doi.org/10.1080/15476278.2015.1019687.
[58] Y. Liu, Z. Li, J. Li, S. Yang, Y. Zhang, B. Yao, W. Song, X. Fu, S. Huang, Stiffness-mediated mesenchymal stem cell fate decision in 3D-bioprinted hydrogels, Burns Trauma 8 (2021), https://doi.org/10.1093/BURNST/TKAA029.
[59] R.S. Navarro, M.S. Huang, J.G. Roth, K.M. Hubka, C.M. Long, A. Enejder, S. C. Heilshorn, Tuning polymer hydrophilicity to regulate gel mechanics and encapsulated cell morphology, Adv. Healthc. Mater. 11 (13) (2022), https://doi.org/10.1002/adhm.202200011.
[60] J. Wei, J. Yao, C. Yang, Y. Mao, D. Zhu, Y. Xie, P. Liu, M. Yan, L. Ren, Y. Lin, Q. Zheng, X. Li, Heterogeneous matrix stiffness regulates the cancer stem-like cell phenotype in hepatocellular carcinoma, J. Transl. Med. 20 (1) (2022), https://doi.org/10.1186/s12967-022-03778-w.
[61] T. Yeung, P.C. Georges, L.A. Flanagan, B. Marg, M. Ortiz, M. Funaki, N. Zahir, W. Ming, V. Weaver, P.A. Janmey, Effects of substrate stiffness on cell morphology, cytoskeletal structure, and adhesion, Cell Motil. Cytoskeleton 60 (1) (2005) 24–34, https://doi.org/10.1002/cm.20041.
[62] A.J. Engler, S. Sen, H.L. Sweeney, D.E. Discher, Matrix elasticity directs stem cell lineage specification, Cell 126 (4) (2006) 677–689, https://doi.org/10.1016/j.cell.2006.06.044.
[63] A. Kolipaka, P.A. Wassenaar, S. Cha, W.M. Marashdeh, X. Mo, P. Kalra, B. Gans, B. Raterman, E. Bourekas, Magnetic resonance elastography to estimate brain stiffness: measurement reproducibility and its estimate in pseudotumor cerebri patients, Clin. Imaging 51 (2018) 114–122, https://doi.org/10.1016/j.clinimag.2018.02.005.
[64] C. Wang, X. Tong, F. Yang, Bioengineered 3D brain tumor model to elucidate the effects of matrix stiffness on glioblastoma cell behavior using peg-based hydrogels, Mol. Pharm. 11 (7) (2014) 2115–2125, https://doi.org/10.1021/mp5000828.
[65] A. Alsebaey, N. Allam, K. Alswat, I. Waked, Normal liver stiffness: a study in living donors with normal liver histology, World J. Hepatol. 7 (8) (2015) 1149–1153, https://doi.org/10.4254/wjh.v7.i8.1149.
[66] A. Ravichandran, B. Murekatete, D. Moedder, C. Meinert, L.J. Bray, Photocrosslinkable liver extracellular matrix hydrogels for the generation of 3D liver microenvironment models, Sci. Rep. 11 (1) (2021), https://doi.org/10.1038/s41598-021-94990-z.
[67] H. Maruyama, Y. Yokota, K. Hosono, F. Arai, Hydrogel heart model with temperature memory properties for surgical simulation, Sensors 19 (5) (2019), https://doi.org/10.3390/s19051102.
[68] S. Krishnamoorthy, B. Noorani, C. Xu, Effects of encapsulated cells on the physical–mechanical properties and microstructure of gelatin methacrylate hydrogels, Int. J. Mol. Sci. 20 (2019) 5061, https://doi.org/10.3390/ijms20205061.
[69] Q.L. Loh, C. Choong, Three-dimensional scaffolds for tissue engineering applications: role of porosity and pore size, Tissue Eng. Part B Rev. 19 (2013) 485–502, https://doi.org/10.1089/ten.teb.2012.0437.
[70] N. Annabi, J.W. Nichol, X. Zhong, C. Ji, S. Koshy, A. Khademhosseini, F. Dehghani, Controlling the porosity and microarchitecture of hydrogels for tissue engineering, Tissue Eng. Part B Rev. 16 (2010) 371–383, https://doi.org/10.1089/ten.teb.2009.0639.
[71] L. Bova, F. Maggiotto, S. Micheli, M. Giomo, P. Sgarbossa, O. Gagliano, D. Falcone, E. Cimetta, A porous gelatin methacrylate-based material for 3D cell-laden constructs, Macromol. Biosci. 23 (2023) 2200357, https://doi.org/10.1002/mabi.202200357.
[72] Z. Chen, Y. Lv, Gelatin/sodium alginate composite hydrogel with dynamic matrix stiffening ability for bone regeneration, Compos. Part B Eng. 243 (2022), https://doi.org/10.1016/j.compositesb.2022.110162.
[73] H. Wen, W. Xiao, S. Biswas, Z.Q. Cong, X.M. Liu, K.S. Lam, Y.H. Liao, W. Deng, Alginate hydrogel modified with a ligand interacting with α3β1 integrin receptor promotes the differentiation of 3D neural spheroids toward oligodendrocytes in

vitro, ACS Appl. Mater. Interfaces (2019), https://doi.org/10.1021/acsami.8b19438.
[74] Y. Lee, J.M. Lee, P.-K. Bae, I.Y. Chung, B.H. Chung, B.G. Chung, Photo-crosslinkable hydrogel-based 3D microfluidic culture device, ELECTROPHORESIS 36 (7–8) (2015) NA–NA, https://doi.org/10.1002/elps.201570071.
[75] Lei Zhou, Lei Fan, Feng-Miao Zhang, Yuhe Jiang, Min Cai, Cong Dai, Yi-An Luo, Ling-Jie Tu, Zheng-Nan Zhou, Xiao-Jun Li, Cheng-Yun Ning, Kai Zheng, Aldo R. Boccaccini, Guo-Xin Tan, Hybrid gelatin/oxidized chondroitin sulfate hydrogels incorporating bioactive glass nanoparticles with enhanced mechanical properties, mineralization, and osteogenic differentiation, Bioact. Mater. (2021) 890–904.
[76] J.P. Mazzoccoli, D.L. Feke, H. Baskaran, P.N. Pintauro, Mechanical and cell viability properties of crosslinked low- and high-molecular weight poly(ethylene glycol) diacrylate blends, J. Biomed. Mater. Res. A. 93 (2) (2010) 558–566, https://doi.org/10.1002/jbm.a.32563.
[77] Z. Wu, Q. Li, S. Xie, X. Shan, Z. Cai, In vitro and in vivo biocompatibility evaluation of a 3D bioprinted gelatin-sodium alginate/rat Schwann-cell scaffold, Mater. Sci. Eng. C 109 (2020), https://doi.org/10.1016/j.msec.2019.110530.
[78] A. Lavrentieva, M. Kirsch, L. Birnstein, I. Pepelanova, W. Handke, J. Rach, A. Seltsam, T. Scheper, Gelatin-methacryloyl (GelMA) formulated with human platelet lysate supports mesenchymal stem cell proliferation and differentiation and enhances the hydrogel's mechanical properties, Bioengineering 6 (3) (2019), https://doi.org/10.3390/bioengineering6030076.
[79] I. Pepelanova, K. Kruppa, T. Scheper, A. Lavrentieva, Gelatin-methacryloyl (GelMA) hydrogels with defined degree of functionalization as a versatile toolkit for 3D cell culture and extrusion bioprinting, Bioengineering 5 (3) (2018), https://doi.org/10.3390/bioengineering5030055.
[80] D.F. Mangan, G.R. Welch, S.M. Wahl, Lipopolysaccharide, tumor necrosis factor-cy, and IL-1/3 prevent programmed cell death (apoptosis) in human peripheral blood monocytes'. http://journals.aai.org/jimmunol/article-pdf/146/5/1541/1051836/1541.pdf, 1991.
[81] J. Bystroňová, I. Ščigalková, L. Wolfová, M. Pravda, N.E. Vrana, V. Velebný, Creating a 3D microenvironment for monocyte cultivation: ECM-mimicking hydrogels based on gelatine and hyaluronic acid derivatives, RSC Adv. 8 (14) (2018) 7606–7614, https://doi.org/10.1039/c7ra13739g.
[82] V. Walf-Vorderwülbecke, K. Pearce, T. Brooks, M. Hubank, M.M. Van Den Heuvel-Eibrink, C.M. Zwaan, S. Adams, D. Edwards, J. Bartram, S. Samarasinghe, P. Ancliff, A. Khwaja, N. Goulden, G. Williams, J. De Boer, O. Williams, Targeting acute myeloid leukemia by drug-induced c-MYB degradation, Leukemia 32 (4) (2018) 882–889, https://doi.org/10.1038/leu.2017.317.
[83] J. Kim, C.M. Hope, N. Gantumur, G.B. Perkins, S.O. Stead, Z. Yue, X. Liu, A. U. Asua, F.D. Kette, D. Penko, C.J. Drogemuller, R.P. Carroll, S.C. Barry, G. G. Wallace, P.T. Coates, Encapsulation of human natural and induced regulatory T-cells in IL-2 and CCL1 supplemented alginate-GelMA hydrogel for 3D bioprinting, Adv. Funct. Mater. 30 (15) (2020), https://doi.org/10.1002/adfm.202000544.
[84] N. Shah, P.M. Hallur, R.A. Ganesh, P. Sonpatki, D. Naik, K.P. Chandrachari, R. B. Puchalski, A. Chaubey, Gelatin methacrylate hydrogels culture model for glioblastoma cells enriches for mesenchymal-like state and models interactions with immune cells, Sci. Rep. 11 (1) (2021), https://doi.org/10.1038/s41598-021-97059-z.
[85] F. Mousawi, H. Peng, J. Li, S. Ponnambalam, S. Roger, H. Zhao, X. Yang, L. H. Jiang, Chemical activation of the Piezo1 channel drives mesenchymal stem cell migration via inducing ATP release and activation of P2 receptor purinergic signaling, Stem Cells 38 (3) (2020) 410–421, https://doi.org/10.1002/stem.3114.
[86] Pittenger, M. F., Mackay, A. M., Beck, S. C., Jaiswal, R. K., Douglas, R., Mosca, J. D., Moorman, M. A., Simonetti, D. W., Craig, S., & Marshak, D. R. (1987). 10. C. Zener. In J. Electrochem. Soc (Vol. 58, issue 2). Academic press. www.sciencemag.org/feature/.
[87] X. Fu, G. Liu, A. Halim, Y. Ju, Q. Luo, G. Song, Mesenchymal stem cell migration and tissue repair, Cells 8 (8) (2019), https://doi.org/10.3390/cells8080784.
[88] A. Infante, C.I. Rodríguez, Osteogenesis and aging: lessons from mesenchymal stem cells, Stem Cell Research & Therapy 9 (1) (2018) 244. NLM (Medline), https://doi.org/10.1186/s13287-018-0995-x.
[89] O. Al-Jaibaji, S. Swioklo, K. Gijbels, B. Vaes, F.C. Figueiredo, C.J. Connon, Alginate encapsulated multipotent adult progenitor cells promote corneal stromal cell activation via release of soluble factors, PloS One 13 (9) (2018), https://doi.org/10.1371/journal.pone.0202118.
[90] S. Swioklo, A. Constantinescu, C.J. Connon, Alginate-encapsulation for the improved hypothermic preservation of human adipose-derived stem cells, Stem Cells Transl. Med. 5 (3) (2016) 339–349, https://doi.org/10.5966/sctm.2015-0131.
[91] C.T.J. van Velthoven, T.A. Rando, Stem cell quiescence: dynamism, restraint, and cellular idling, Cell Stem Cell 24 (2) (2019) 213–225, https://doi.org/10.1016/j.stem.2019.01.001.
[92] N.S. Lewis, E.E.L. Lewis, M. Mullin, H. Wheadon, M.J. Dalby, C.C. Berry, Magnetically levitated mesenchymal stem cell spheroids cultured with a collagen gel maintain phenotype and quiescence, Journal of Tissue Engineering 8 (2017), https://doi.org/10.1177/2041731417704428.
[93] D. Lü, C. Luo, C. Zhang, Z. Li, M. Long, Differential regulation of morphology and stemness of mouse embryonic stem cells by substrate stiffness and topography, Biomaterials 35 (13) (2014) 3945–3955, https://doi.org/10.1016/j.biomaterials.2014.01.066.
[94] V.O.C. Rigaud, R. Hoy, S. Mohsin, M. Khan, Stem cell metabolism: powering cell-based therapeutics, Cells 9 (11) (2020), https://doi.org/10.3390/cells9112490.
[95] X.L. Wang, J.T. Jiang, C.P. Wu, Prognostic significance of tumor-associated macrophage infiltration in gastric cancer: a meta-analysis, Genet. Mol. Res. 15 (4) (2016), https://doi.org/10.4238/GMR15049040.
[96] S.B. Anderson, C.C. Lin, D.V. Kuntzler, K.S. Anseth, The performance of human mesenchymal stem cells encapsulated in cell-degradable polymer-peptide hydrogels, Biomaterials 32 (14) (2011) 3564–3574, https://doi.org/10.1016/j.biomaterials.2011.01.064.
[97] A.H. Aziz, S.J. Bryant, A comparison of human mesenchymal stem cell osteogenesis in poly(ethylene glycol) hydrogels as a function of MMP-sensitive crosslinker and crosslink density in chemically defined medium, Biotechnol. Bioeng. 116 (6) (2019) 1523–1536, https://doi.org/10.1002/bit.26957.
[98] T.J. Bartosh, J.H. Ylostalo, Preparation of anti-inflammatory mesenchymal stem/precursor cells (MSCs) through sphere formation using hanging-drop culture technique, Curr. Protoc. Stem Cell Biol. 1 (SUPPL.28) (2014), https://doi.org/10.1002/9780470151808.sc02b06s28.
[99] N.E. Ryu, S.H. Lee, H. Park, Spheroid culture system methods and applications for mesenchymal stem cells, Cells 8 (12) (2019), https://doi.org/10.3390/cells8121620.
[100] Y.C. Tung, A.Y. Hsiao, S.G. Allen, Y.S. Torisawa, M. Ho, S. Takayama, High-throughput 3D spheroid culture and drug testing using a 384 hanging drop array, Analyst 136 (3) (2011) 473–478, https://doi.org/10.1039/c0an00609b.
[101] E.M. Kim, Y. bin Lee, S. jeong Kim, J. Park, J. Lee, S.W. Kim, H. Park, H. Shin, Fabrication of core-shell spheroids as building blocks for engineering 3D complex vascularized tissue, Acta Biomater. 100 (2019) 158–172, https://doi.org/10.1016/j.actbio.2019.09.028.
[102] S.S. Ho, K.C. Murphy, B.Y.K. Binder, C.B. Vissers, J.K. Leach, Increased survival and function of mesenchymal stem cell spheroids entrapped in instructive alginate hydrogels, Stem Cells Transl. Med. 5 (6) (2016) 773–781, https://doi.org/10.5966/sctm.2015-0211.
[103] Q. Zhang, A.L. Nguyen, S. Shi, C. Hill, P. Wilder-Smith, T.B. Krasieva, A.D. Le, Three-dimensional spheroid culture of human gingiva-derived mesenchymal stem cells enhances mitigation of chemotherapy-induced oral mucositis, Stem Cells Dev. 21 (6) (2012) 937–947, https://doi.org/10.1089/scd.2011.0252.
[104] E. Gheytanchi, M. Naseri, F. Karimi-Busheri, F. Atyabi, E.S. Mirsharif, M. Bozorgmehr, R. Ghods, Z. Madjd, Morphological and molecular characteristics of spheroid formation in HT-29 and Caco-2 colorectal cancer cell lines, Cancer Cell Int. 21 (1) (2021), https://doi.org/10.1186/s12935-021-01898-9.
[105] A. Imamura, H. Kajiya, S. Fujisaki, M. Maeshiba, T. Yanagi, H. Kojima, J. Ohno, Three-dimensional spheroids of mesenchymal stem/stromal cells promote osteogenesis by activating stemness and Wnt/β-catenin, Biochem. Biophys. Res. Commun. 523 (2) (2020) 458–464, https://doi.org/10.1016/j.bbrc.2019.12.066.
[106] Z. Cesarz, K. Tamama, Spheroid culture of mesenchymal stem cells, Stem Cells Int. 2016 (2016), https://doi.org/10.1155/2016/9176357.
[107] R.Z. Lin, H.Y. Chang, Recent advances in three-dimensional multicellular spheroid culture for biomedical research, Biotechnol. J. 3 (9–10) (2008) 1172–1184, https://doi.org/10.1002/biot.200700228.
[108] C. Liu, D. Lewin Mejia, B. Chiang, K.E. Luker, G.D. Luker, Hybrid collagen alginate hydrogel as a platform for 3D tumor spheroid invasion, Acta Biomater. 75 (2018) 213–225, https://doi.org/10.1016/j.actbio.2018.06.003.
[109] K.B. Fonseca, F.R. Maia, F.A. Cruz, D. Andrade, M.A. Juliano, P.L. Granja, C. C. Barrias, Enzymatic, physicochemical and biological properties of MMP-sensitive alginate hydrogels, Soft Matter 9 (12) (2013) 3283–3292, https://doi.org/10.1039/c3sm27560d.